Summary to the reply and manuscript revision

The authors would like to sincerely thank the two anonymous referees for the review of the original manuscript, and the discussion involved in the process. We consider these suggestions and comments invaluable for improving the manuscript's relevance and quality. There is a common question by both referees on the potential of circular reasoning and the independency of the data during verifications. In this summary, we would like to address this common question. For other specific comments, the replies are provided by compilation of reply documents to all the available commentary documents (RC1 to RC3).

Concerning the common question of the potential of circular reasoning and the independency of the data, we would like to provide the following proof. **First**, without the covariability, the retrieval can still be carried out by using mean $\boldsymbol{FB_{snow}}$ and L-band TB, and with the covariability info that supports multiple $\boldsymbol{FB_{snow}}$ samples, the quality of retrieval is improved for both ***hi*** and ***hs***. This shows that covariability ONLY plays a central role in general retrieval problem which involves high-resolution altimetry samples and (relatively) low resolution L-band radiometry. The evidence is now added in the revised manuscript (pg. 10, l. 31 to pg. 11, l. 6).

Second, without TB, the "retrieval" can be achieved with ONLY the covariability (by using the mean values for *alpha* and *beta*), BUT the quality of retrieval is much compromised, especially for ***hs***. This indicates that TB plays an important role in the combined retrieval process. The quantitative results are provided in the foremost part of the reply to RC3.

Third, with respect to the data dependency in the derivation of ***s*** (the parameter that characterize covariability), we divide the OIB data by years. According to the suggestion from referee #1, the values of ***s*** as derived from years before 2015 are used for the retrieval for OIB data in 2015 (to ensure independency). The results (shown in reply document to RC2) show that the retrieval can be carried out for data in 2015, with comparable performance for both ***hi*** and ***hs***.

Fourth, the accurately modeled TB ensures good retrieval, and whether the sea ice cover is sufficiently surveyed by altimetry scans plays an important role in the TB error (RMSE of TB dropping from 3.1 K for all data to 1.4 K for well-scanned areas). Quantitative result of TB error is provided in the supplementary material (as well as reply to RC3), and the effects on retrieval in the revised manuscript (pg. 10, l. 20 to l. 31).

The specific replies and the revised manuscript are provided after this summary. The contents of the following parts are outlined as followings. Within each part of the content, the figures and references are numbered and provided independently. The highlighted parts in the revised manuscript differs by color: the revisions according to the first referee's comments (RC1 and RC2) are in yellow, and those to the second referee's (RC3) are in green.

The authors sincerely hope that the contents of the manuscript are fully and accurately conveyed, and would like very much to reply any further potential questions from the referees and the editor.

Contents:

Reply to RC1:

The authors thank the referee #1 for the review and suggestion to our manuscript. We would like to make the following clarifications and responses to the comments.

***Comment from the referee**:*
The authors use laser-based snow freeboard and radar-based snow thickness as well as the sea ice thickness from OIB flights. One problem of the present manuscript arises from the fact that the sea ice thickness in the OIB product was derived using the snow freeboard and the radar-based snow thickness (Kurtz et al., 2013). Therefore, it is not very surprising that the authors find a very high covariance between snow depth, thickness and freeboard because the quantities can not be considered as results from independent measurements. The "verification" in Figure 7 seems to just exemplify this circular reasoning. Additional problems arises from the fact that different snow depth algorithms for OIB exist and that the instrumentation has changed from year to year (Kwok et al., 2017). The dependency of the used data sets and the lack of discussion of the used assumptions cast serious doubts on the validity of the conclusions.

Concerning the judgment by the referee that the verification in the manuscript is "circular reasoning", we would like to point out that the verification is carried out based on the data independent from what used in the retrieval process. **Three clarifications are provided as follows.**

1. **Data independency in the covariability analysis.** Although the OIB data is used in the analysis, the covariability is carried out between two independently measured parameters: **the total freeboard** measured by airborne topographic mapper (ATM), and **snow depth** measured by ultra-wideband frequency-modulated continuous-wave (FMCW) radar (see Farrell et al., 2012 and related references). Thus the two observations can be considered as independent. Moreover, the covariability analysis is **NOT** carried out between the freeboard (or snow depth) and sea ice thickness, since sea ice thickness is a derived parameter based on the hydrostatic equilibrium relationship. Note that sea ice thickness of OIB is only used in the verification of the retrieved parameters.

2. **Covariability between snow depth and total freeboard is physically sound, and NOT due to that they are not independent.** Considering Equation 1 of the manuscript (isostatic equilibrium model) which relates snow depth, sea ice thickness and the total freeboard, the relationship can be expressed as follows (using the notation in the manuscript):

$$FB_s = \frac{\rho_w - \rho_i}{\rho_w} \cdot h_i + \frac{\rho_w - \rho_s}{\rho_w} \cdot h_s \approx 0.1 \cdot h_i + 0.67 \cdot h_s$$

As indicated by this relationship, if the value of snow depth is considered a random variable, the value of the total freeboard (also a random variable) is clearly correlated with it. Therefore, this covariability is inherent in the physics, NOT due to the data collection process (or OIB in this case). See also Kwok et al., (2011) (subfigure d of figure 10, 11 and 12) for a similar analysis which also provides justification of covariability, but on a different spatial scale of 4 km.

3. **Role of the covariability in the retrieval.** The covariability (between snow depth and total freeboard) is a statistical relationship derived from the OIB data, and the parameters derived from functional fitting (see Section 3.1) using basin-wide observations that are integrated into the retrieval. During the retrieval, the input data include the total freeboard and the L-band TB, and the output data are sea ice thickness and snow depth, while the covariability (in terms of the fitted parameters) serves as a supportive info. The only place where the local information of covariability is used is in the analysis of the sources of the

retrieval error in Section 3.2 and Section 4. During the actual retrieval, the local covariability information is NOT available, and Figure 7c and d shows that the corresponding retrieval results are in good consistency with the observed sea ice parameters. Therefore, to summarize the proofs, for the design of the retrieval algorithms and the verification, we does not consider there exists circular reasoning.

Second, concerning the quality of the OIB data especially the snow depth algorithms applied for each year, we make the following explanations of the details of OIB data used in the analysis. In Kwok et al. (2017) (also the reference provided by the referee), five retrieval algorithms (NISDC, GSFC-NK, SLRD, Wavelet, JPL) for snow depth in OIB are discussed. In these five algorithms, both NISDC and GSFC-NK retrievals have lower scatter compared to in situ campaigns and large inter-annual variability compared to the climatological fields. Kurtz et al., (2013a) indicates that IDSI4 product are capable of providing a reliable record of snow depth through independent data comparison. For our analysis and validation, we use IDSI4 dataset in 2009-2013 (Kurtz et al., 2015), which is the existing NSIDC product, and quick-look dataset in 2014–2016, which is based on GSFC-NK algorithm. Data from the quick-look data is used for the campaign which is not accessible since 2014. Quick-look product, which uses modified algorithms to minimize freeboard biases (Kurtz, 2013; Kurtz et al., 2014), takes the consideration of different instrument characteristics of the snow radar. Despite that it is possible that the uncertainties in this product are higher than in IDSI4 product (Kurtz et al., 2013b), we consider the data product as used in the manuscript are optimum in terms of the overall small bias and good consistency with in-situ measurements, for the purpose of the analysis of covariability and the verification of the retrieval algorithm.

Third, we want to emphasize that the main purpose of the manuscript is the introduction of the retrieval methodology, and the demonstration of its validity through verification with OIB data. Since the "true" values of both snow depth and sea ice thickness are available from OIB, we use the total freeboard measurements (to simulate satellite laser altimetry) and SMOS TB data for the retrieval and verification with the aforementioned "true" or reference values of OIB. Similar practice of using OIB data for verifications to the retrieval algorithm is also common. Take Maaß et al. (2013) as an example. The snow depth from OIB is used to verify the retrieved snow depth (figure 9 and 10), while the sea ice thickness from OIB is used to guarantee the prerequisite of the retrieval algorithm that the sea ice is thick enough. With respect to the data production with actual satellite data, the covariability that is specific to the resolution of the satellite altimetry should be used (which can be potentially derived from OIB data due to the higher resolution) and compared against other independent data sources for verification, such as other campaigns. We consider this an important direction of future work, which is beyond the length and scope of current work.

***Comment from the referee**:*

Regarding the use of L-band brightness temperatures I found the Figure 1 misleading with emissions arising just from the surface and not from the ice volume or deeper layers. Some crucial model assumptions are not explained in the manuscript, e.g. the parameterization of ice salinity. It seems that a thickness dependent parameterization was used otherwise I can not explain the large sensitivity to ice thickness exceeding 3 meter. All this should be explained and discussed in the manuscript. This is perhaps described in the reference Zhou et al. (accepted) but is not yet available to me.

First, concerning the misleading plot (Figure 1), our original intention is to contrast the altimetry and passive remote sensing techniques. Here we modified the figure to avoid the unnecessary misleading info. The modified figure is shown below.

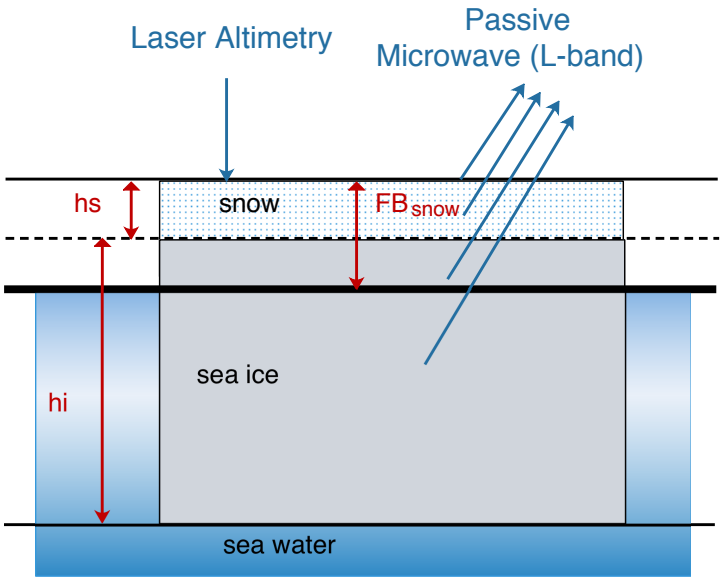

Modified figure 1. Schematic view of sea ice parameters and active/passive remote sensing of the sea ice cover. The parameters include sea ice thickness (hi), snow depth (hs) and snow freeboard (FBsnow).

Second, concerning the L-band radiation model used for the retrieval, the model is a multi-layer radiation model based on sea ice type-dependent salinity and temperature profile. The model is verified using OIB and SMOS observational datasets. The manuscript documenting the radiation model has been accepted by International Journal of Remote Sensing (Zhou et al., 2017), but it is not available for public at this moment. Here we would like to quote relevant description of the model and the accompanying figure as below. Please also see Section 2.3 and Figure 3.a (salinity profile) for other supportive information.

> *"In order to explore the sensitivity of the L-band radiation model to the properties of sea ice, we reformulate the model to include multiple layers for sea ice and snow, instead of a single layer adopted by Maass et al. (2013). Specifically, we use a linear vertical temperature prole for the sea ice and snow, based on prescribed thermal conductivity of sea ice and snow, following Untersteiner (1964) and Yu and Rothrock (1996).*
>
> *…-*
>
> *Furthermore, we distinguish the difference in salinity between first-year ice (FYI) and multi-year ice (MYI). For FYI, following Cox and Weeks (1974), a constant salinity prole based on the ice thickness is used to characterize the fact that the salinity has not drained. For MYI, a salinity prole based on observations is used to reflect the effect of brine drainage and flushing during the melt season.*
>
> *…*
>
> *We denote the original model as the single layer radiation model as adopted in Maass et al. (2013), and the improved model as the multi-layer model with ice type dependent vertical temperature and salinity prole. Figure 4.a shows the scatterplot between the original modeled and SMOS observed T_B for 22 Mar 2012, while Figure 4.b is for the improved model. The original modeled T_B tends to cluster around 250K, irrespective of the large range of observed T_B values (y-axis). Clearly, the improved model produces a much better t than that of the original model (0.84 as compared to 0.60 for R^2). The overestimated T_B by the original model for both FYI (triangles) and MYI (circles) are significantly reduced. Figure 4.c (4.d) show the scatterplot for 18 Mar 2014 and 1 Apr 2015 under the original model (the improved model). Again, the simulated T_B is in much better agreement with observations (0.01 as compared to 0.68 for R^2). Taking a close look at Figure 4.b and 4.d, we note that the simulated T_B on 18 Mar 2014 and 1 Apr 2015 is not tightly clustered along the t line as that of 22 Mar 2012, which is also reflected by the relatively lower R^2 in Figure 4.d as compared to Figure 4.b. For these two days, there exist extensive leads as observed by OIB campaigns, which are small in width and not directly distinguishable by L-band observations of SMOS.*

…"

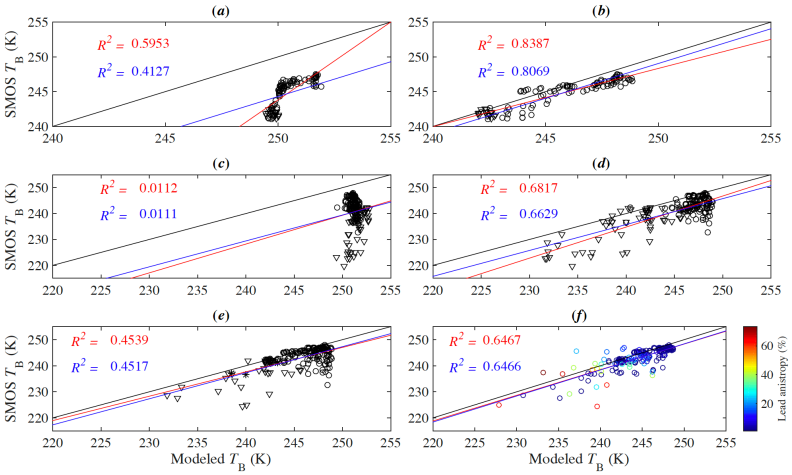

Figure 4. Comparison of modeled and observed T_B for OIB data from representative days. Subfigure *a* to *d* compares the original model and the improved model (with the multi-layer formulation and the vertical salinity and temperature profile). Subfigure *a* (or *c*) and *b* (or *d*) show the evaluation of the original model and the improved model for 22 Mar 2012 with no presence of sea ice leads on the OIB track (or 18 Mar 2014 and 1 Apr 2015 with the OIB tracks covering sea ice leads). The effect of the integration of MODIS lead map is further compared by subfigure *e* (with the improved model but without lead information) and *f* (with lead information). FYI and MYI are marked out by triangles and circles, respectively. Red lines are the least square fit, whilst blue lines are the least square under the constraint that the slope of the fit line is 1. Black lines are 1:1 lines.

We would also like to provide the accepted manuscript (Zhou et al., 2017) to the referee upon request. Furthermore, we want to emphasize the sensitivity for sea ice over 3 meters thick arises from that the retrieval of ice thickness is based on the total freeboard and L-band TB. The referee is kindly directed to Figure 3c, in which the relationship between the L-band TB and sea ice parameters is shown. The retrieval is carried out under a certain total freeboard value (shown by green constant-freeboard lines in the figure), but a certain snow depth. Therefore, even the TB saturates when sea ice is thick under a prescribed snow depth (black lines in Figure 3c), for the proposed algorithm there still exists good retrievability. Section 2.3 (line 26 on page 5) gives a more thorough description on this issue.

***Comment from the referee**:*

Another issue with the manuscript is the overall aim of the method. It is not yet clear what is the main advantage of combining laser altimetry and L-band radiometry? Is the method for the fusion of airborne and satellite data or for to be used for future satellite missions? For the ICESat period there are no L-band radiometer data available. For the ICESat-2 period it is not clear if SMOS and/or SMAP are still in operation. What about the different spatial and temporal samplings and uncertainties? These practical considerations are not yet even mentioned.

First, concerning the advantage of the proposed retrieval algorithm, we would like to further emphasize the status-quo of the retrieval of snow depth and sea ice thickness (see also Section 1, the second and the third paragraph). Current retrieval algorithms mainly focus on a single type of sea ice parameter (such as ice thickness or snow depth), and thus exists large uncertainty due to the lack of knowledge of other parameters. The aim of the proposed algorithm is to retrieve both parameters simultaneously, without simple assumptions such as the snow depth estimations (from climatology or reanalyses) in laser altimetry. The retrieved parameters should be able to serve as better estimations of these parameters and serve potential climatological and operational usage.

Second, concerning the retrieval with simultaneous satellite campaigns, we mainly target at the synergy of observational data between ICESat-2 and SMOS/SMAP. The manuscript provides a basis for the retrieval algorithm design with actual satellite data. ICESat-2 is currently scheduled for launch in 2018

(see https://icesat-2.gsfc.nasa.gov). SMOS and SMAP have been in service since late 2009 and early 2015. Although the designed lifespan of SMOS and SMAP are both 3 years, it is worth noting that SMOS have been providing service for over 7 years. Since it is invaluable for the availability of satellites that co-register the interested regions with complementary capabilities, we would like to express their optimism in the satellite campaigns and determination to make better usage of potential data for the retrieval of sea ice parameters. Additionally, the ongoing Chinese satellite campaign WCOM (Shi et al., 2016) with passive microwave remote sensing (including L-band) capabilities will cover the Arctic region, which serves as another candidate dataset. WCOM is scheduled to launch before 2020. For the co-registration of WCOM and ICESat-2, the combined retrieval can be carried out for the corresponding total freeboard and L-band TB measurements.

***Comment from the referee**:*

P4L7 The resolution of the radiometer depends mainly on the size of the antenna.

According to the comment, the authors have made the correction to the manuscript with respect to the resolution of radiometry.

References:

Kwok R, Kurtz N T, Brucker L, et al. Inter-comparison of snow depth retrievals over Arctic sea ice from radar data acquired by Operation IceBridge. Cryosphere Discussions, 2017:1-37.

Kwok, R., Panzer, B., Leuschen, C., Pang, S., Markus, T., Holt, B., and Gogineni, S.: Airborne surveys of snow depth over Arctic sea ice, Journal of Geophysical Research: Oceans, 116, 2011.

Kurtz, N.: IceBridge quick look sea ice freeboard, snow depth, and thickness product manual for 2013, Boulder, Colorado USA: NASA DAAC at the National Snow and Ice Data Center, 2013.

Kurtz N T, Farrell S L, Studinger M, et al. Sea ice thickness, freeboard, and snow depth products from Operation IceBridge airborne data. Cryosphere, 2013a, 7(4):1035-1056.

Kurtz N, Richter-Menge J, Farrell S, et al. IceBridge Airborne Survey Data Support Arctic Sea Ice Predictions[J]. Eos Transactions American Geophysical Union, 2013b, 94(4):41-41.

Kurtz N T, Galin N, Studinger M. An improved CryoSat-2 sea ice freeboard retrieval algorithm through the use of waveform fitting. Cryosphere, 2014, 8(1):1217-1237.

Kurtz, N., Studinger, M., Harbeck, J. P., Onana, V. D., and Yi, D.: IceBridge L4 Sea Ice Freeboard, Snow Depth, and Thickness, Version 1, Boulder, Colorado USA., NASA National Snow and Ice Data Center Distributed Active Archive Center., doi: 10.5067/G519SHCKWQV6, 2015. 2015.

Maaß, N., Kaleschke, L., Tian-Kunze, X., and Drusch, M.: Snow thickness retrieval over thick Arctic sea ice using SMOS satellite data, The Cryosphere, 2013, 7, 1971–1989, doi:10.5194/tc-7-1971-2013..

J. Shi, X. Dong, T. Zhao, Y. Du, H. Liu, Z. Wang, D. Zhu, D. Ji, C. Xiong, L. Jiang. The water cycle observation mission (WCOM): Overview. 2016 IEEE International Geoscience and Remote Sensing Symposium (IGARSS), Beijing, 2016, pp. 3430-3433, doi: 10.1109/IGARSS.2016.7729886

Sinéad Louise Farrell, Nathan Kurtz, Laurence N. Connor, Bruce C. Elder, Carlton Leuschen, Thorsten Markus, David C. McAdoo, Ben Panzer, Jacqueline Richter-Menge, and John G. Sonntag. A First Assessment of IceBridge Snow and Ice Thickness Data Over Arctic Sea Ice, IEEE Transactions on Geoscience and Remote Sensing, Vol 50, No 6, 2012.

Lu Zhou, Shiming Xu, Jiping Liu, Hui Lu and Bin Wang, Improving L-Band Radiation Model and Representation of Small-Scale Variability to Simulate Brightness Temperature of Sea Ice, accepted by International Journal of Remote Sensing, doi: 10.1080/01431161.2017.1371862.

Reply to RC2:

The authors would like to thank the referee for the prompt and precise comments to our reply. We have made modifications and the accompanying reply as follows.

The referee's comments:

Thank you for the rebuttal and providing the additional reference to the publication in the International Journal of Remote Sensing. The idea with the combination of lead data is very good. However, after reading the other paper even more questions arose because the publication also lacks traceability. I would not be able to reproduce your results with the somehow limited information given in the paper. Really important information is missing, some details are even wrong. For example, the used permittivity is not even mentioned. The native SSMI resolution of the 19 GHz channels used in the NASA-Team algorithm (Cavalieri et al. 1996) is about 69x43 not 10 km.

Reply:

With respect to the comment that key information of the L-band radiation model is not available in Zhou et al. (2017), we consider it necessary to formulate a supplementary to describe the model in detail. Specifically, this supplementary includes introduction to the model, including the multi-layer treatment of salinity and temperature profile, sea ice emissivity and permittivity, etc. The modeled L-band brightness temperature (TB) to a range of sea ice parameters for first-year ice (FYI) is also included (Figure S1.a of the supplement), accompanying that for multi-year ice (MYI) in Figure 3c in the manuscript (also Figure S1.b of the supplementary). This supplementary is provided as a supportive document to the original manuscript, and also attached at the end of this reply document.

The following is a concise answer to the referee's question on the permittivity settings in the model: the permittivity of snow, sea ice and sea water mainly follows that in Maaß, et al., (2013). For sea water, an empirical relationship in Klein and Swift (1977) is adopted assuming salinity of 33 g/kg. For sea ice, the permittivity is related to the brine volume fraction, based on Vant et al. (1978) and specific settings in Kaleschke et al. (2010). For snow, same as Maaß, et al. (2013), we adopt fitted parameterization of permittivity as formulated in Tiuri et al., (1984). For the study in this work, under a multi-layer formulation, the salinity structure of MYI (in terms of salinity for each layer) and its effect on permittivity is characterized. The attached supplement provides details of these model settings.

With respect to the comment that a wrong detail of the native SSMI resolution is present in Zhou et al. (2017), we thank the referee and recognize that this is indeed a mistake. We are preparing a corrigendum to the International Journal of Remote Sensing to correct the description, as indicated by the referee: "*Furthermore, sea ice concentration data as used by this article (Cavalieri et al. 1996) are provided on the resolution of 25 km with the native resolution of about 69 km by 43 km*". For a further reply: other datasets, such as the sea ice concentration based on 89 GHz channel of AMSR-E or AMSR-2 (see Spreen et al., (2008)) serves as candidates for sea ice coverage, which is of about 5 km in nominal resolution. The intention of using sea ice concentration (SIC) in Zhou et al. (2017) is to complement the lead maps in characterizing the effect of (refrozen) open water on the L-band TB of the sea ice cover. Sea ice leads are usually with much small width than the typical passive remote sensing with satellites, and not well represented in the retrieval algorithms for SIC. Therefore, both sea ice lead information and sea ice concentration information are adopted in simulating the TB (see Equation 5 and the last paragraph on page 7075 of Zhou et al., (2017)).

The referee's comments:

Regarding the present manuscript submitted to The Cryosphere, I am still not happy with your answers. I still think you could be fooled by circular reasoning. You should split the data into independent "training" and "test" parts to do a real verification, and this for multi-year and first year ice separately. Thereby the very different resolutions and spatial samplings of the sensors involved have to be carefully considered.

The authors would like to make further clarifications on the issue of circular reasoning, and according to the suggestions of the referee, we carry out experiments with different portion of the dataset and show the results.

First, we would like to clarify that the retrieval is based on the snow freeboard (from OIB) and L-band TB (from SMOS), with L-band radiation model and hydrostatic relationship. The L-band model is not trained to the observations of OIB or SMOS. Besides, the model is qualitatively consistent with existing works such as Maaß et al., (2013). The other supportive information for the retrieval is the covariability between snow depth (***Hs***) and snow freeboard (***FB$_{snow}$***), which is based on OIB data on the spatial scale of 40 meters. However, it is important to note that the covariability in the retrieval is only a generic function shape between ***FB$_{snow}$*** and ***Hs*** (Equation 3 of the manuscript), and this information does NOT directly specify ***Hs*** for any specific ***FB$_{snow}$***. Instead, under the constraints of both observations (***TB*** and ***FB$_{snow}$***), the retrieval algorithm seeks the proper value of α that directly decides ***Hs*** and ***Hi***. Given typical distribution of ***FB$_{snow}$*** for FYI and MYI (in Figure 1.a below), the scanning of α and the resulting mean snow depth are shown in Figure 1.b. The parameter ***s*** that describes the aforementioned covariability (i.e., the function shape parameter) is set to 0.71 and 0.95 for FYI and MYI respectively, which is also adopted in the verification of the original manuscript.

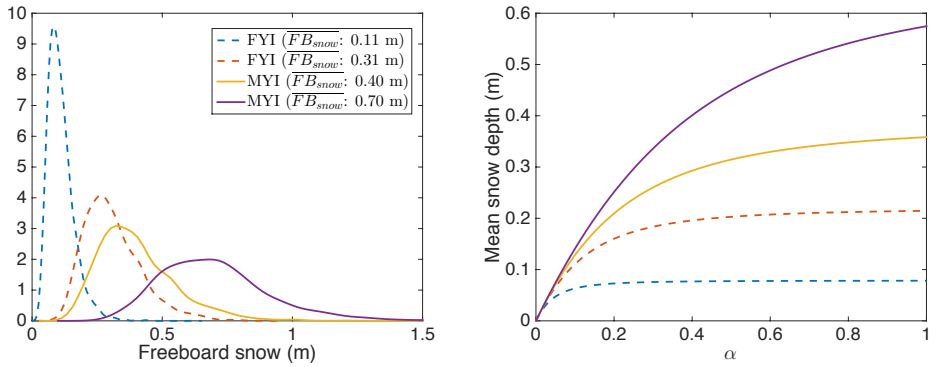

(a) ***FB$_{snow}$*** distribution. (b) Mean snow depth.

Figure 1. Scanning of parameter α and the corresponding mean snow depth.

With respect to the difference in the spatial sampling from various sensors as pointed out by the referee, the authors make the following clarifications on how this difference is accounted for during the retrieval, and analyze the relationship to existing satellite laser altimetry. For the retrieval, we assume that the laser altimetry returns the mean value of ***FB$_{snow}$*** on a certain spatial scale. For example, for ICESat, the spatial scale of each laser scan is about 70 meters, which is different from 40 meters of OIB (L4 data). It is worth noting that covariability between ***Hs*** and ***FB$_{snow}$*** is present on various spatial scales (Kwok et al., (2011)), and there is indeed scaling of the covariability across different scales (i.e., at different resolution for altimetry). Figure 2 (below) shows the distribution of ***s*** derived from all OIB data on various scales, and there is a slight drift of ***s*** to smaller values when manually coarsening the altimetry measurements. This drift applies to both FYI and MYI. Furthermore, in Figure 3 (below), it is shown that there exists distinctive spatial distribution of ***s*** for MYI, with the regions north of the Canadian Archipelago featuring

s>1. Since for the actual retrieval, the local value of ***s*** is not available, in the verification of the original manuscript (Figure 7c and d and corresponding parts), only the global mean value of ***s*** is adopted.

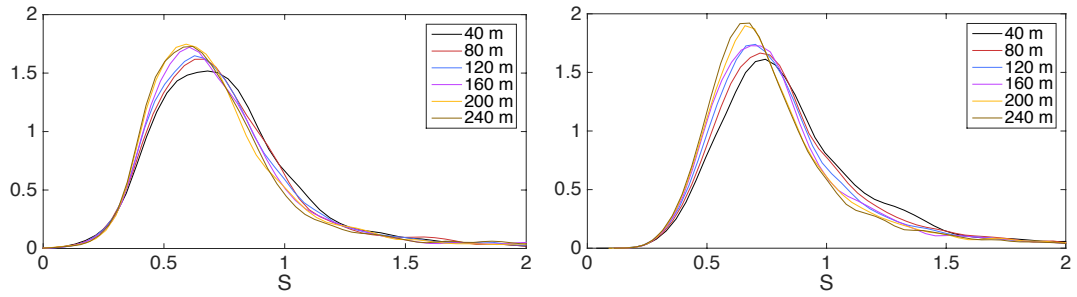

(a) FYI. (b) MYI.

Figure 2. Scaling of ***s*** derived from OIB data.

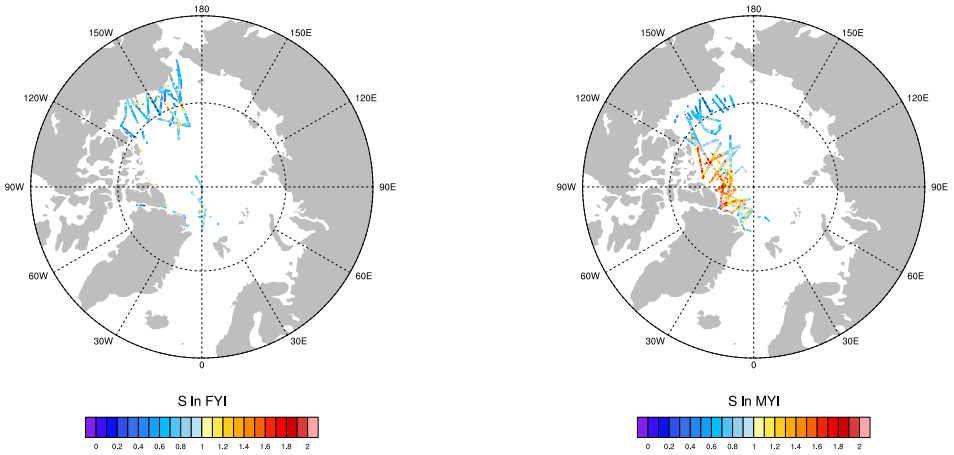

(a) FYI. (b) MYI.

Figure 3. Spatial distribution of ***s***. 40 meter resolution (original OIB) is adopted.

With respect to the suggestions that two separate datasets for "training" and "testing" respectively to ensure independency, the authors have carried out experiments accordingly for further validation of the retrieval. First, the authors would like to clarify that, according to the understanding of the authors, the "training" process mentioned by the referee is the derivation of the value of ***s***. Therefore, we have split all OIB data into years, and use all the data in year 2012 to 2014 to derive ***s*** for FYI and for MYI. This process is denoted "training", and the derived values of ***s*** are 0.73 and 1.00 for FYI and MYI, respectively. These values are applied to the retrieval with OIB data in year 2015 (with $\boldsymbol{FB_{snow}}$ from OIB and SMOS TB), which is denoted the process of "testing". The R^2 of the fitting between the retrieved ***Hi*** (***Hs***) to the observed ***Hi*** (***Hs***) is 0.88 (0.62) for linear fitting and 0.87 (0.61) for linear fitting line with the constraint that the slope be 1, respectively. The results are also shown in Figure 4 (below), which closely resembles those for the large-scale retrieval in the original manuscript (Figure 7c and d). This provides further verification on the consistency of the nonlinear fitting (in terms of ***s***), and that both ***Hi*** and ***Hs*** can be retrieved with the proposed method.

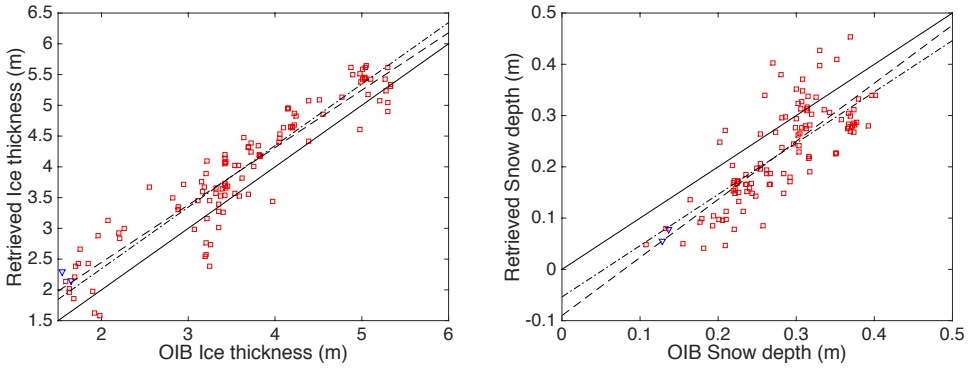

(a) Sea ice thickness. (b) Snow depth.

Figure 4. Verification of retrieval in year 2015. OIB data between 2012 and 2014 are used for the derivation of the values of ***s***. The solid line is the 1:1 line and the dashed (dash-dotted) line represents the linear fitting (linear fitting line with the constraint that the slope be 1)

The authors thank the referee, and consider the referee's comments invaluable in making the manuscript clearer and more relevant. We hope that through the responses above, we can fully convey our idea on the retrieval, and would like to answer potential questions from the referee for further clarification. The materials above (including the supplementary material of the radiation model) are considered by the authors to be merged into the original manuscript in its revised form.

References:

Kaleschke, L., Maaß, N., Haas, C., Hendricks, S., Heygster, G., and Tonboe, R. T.: A sea-ice thickness retrieval model for 1.4 GHz radiometry and application to airborne measurements over low salinity sea-ice, The Cryosphere, 4, 583–592, doi:10.5194/tc-4-583-2010, 2010.

Klein L, Swift C. An improved model for the dielectric constant of sea water at microwave frequencies. IEEE Journal of Oceanic Engineering, 1977, 2(1): 104-111.

Kwok, R., Panzer, B., Leuschen, C., Pang, S., Markus, T., Holt, B., and Gogineni, S.: Airborne surveys of snow depth over Arctic sea ice, Journal of Geophysical Research: Oceans, 116, 2011.

Maaß, N., Kaleschke, L., Tian-Kunze, X., and Drusch, M.: Snow thickness retrieval over thick Arctic sea ice using SMOS satellite data, The Cryosphere, 2013, 7, 1971–1989, doi:10.5194/tc-7-1971-2013.

Spreen, G., L. Kaleschke, and G. Heygster: Sea ice remote sensing using AMSR-E 89 GHz channels. J. Geophys. Res., vol. 113, C02S03, doi:10.1029/2005JC003384.

Vant, M., Ramseier, R., and Makios, V.: The complex-dielectric constant of sea ice at frequencies in the range 0.1–40 GHz, J. Appl. Phys., 49, 1264–1280, 1978.

Zhou, L., S. Xu, J. Liu, H. Lu and B. Wang: Improving L-Band Radiation Model and Representation of Small-Scale Variability to Simulate Brightness Temperature of Sea Ice, International Journal of Remote Sensing, 2017, 38:23, 7070–7084, doi:10.1080/01431161.2017.1371862.

Reply to RC3:

The authors would like to thank the referee for the insightful review of the manuscript and the suggestions for the revision of the manuscript. Replies to the comments by the referee are as follows. The original comments from the referee are shown in italic Arial font, and the reply to each comment is provided immediately after the comment and is in Times font.

Comments A:

The major concerns I have about the presented study are stated here:

*a) The authors do not discuss or show any results at all on the advantage of their suggested approach. If the new contribution here is to combine L-band and altimeter measurements, why do you not show the difference between using this combination of TB and freeboard measurements as compared to just using freeboard measurements and the relationship that you found between snow depth (hs) and FB? This could be done by 1) finding global alpha and beta values (instead of a global s=alpha*beta) and then using these alpha and beta values and Eq. 3 to convert FB to hs and then ice thickness (hi) (using Eq. 1 afterwards) or 2) finding a good fitting formulation that relates hs and hi and then converting FB to hs and hi using Eq. 1. The correlation between FB and hs (R^2=0.67) is very similar to the correlation found between the retrieved and the OIB observed hs for using the global s values and SMOS TBs (R^2=0.64) / simulated TBs (R^2=0.65). Maybe it is essentially the correlation between FB and hs that is behind this agreement of retrieved and observed hs values? From the presented results, I cannot see whether there is any advantage in using L-band additionally...*

The authors would like to emphasize that the main advantage is the simultaneous retrieval of BOTH ***Hi*** and ***Hs***, by combining L-band passive remote sensing and laser altimetry. The covariability information that is incorporated into the retrieval does NOT specify ***Hs***. Rather, this information is only a general constraint between $\boldsymbol{FB_{snow}}$ and ***Hs***. According to the suggestions from the referee, we further carried out "retrieval" study using only the statistics derived from OIB, and NOT using TB. Specifically, the statistics are computed for the parameters ***alpha***, ***beta***, and ***s***. Results are shown in Figure 1 and 2 (below) for FYI and MYI, respectively. Figure 3 (below) shows the retrieval results for ***Hi*** and ***Hs*** using the globally fitted ***alpha*** and ***beta*** on the exactly same spatial scale of the retrieval in the manuscript. The adopted values for these parameters are specific to FYI and MYI: for FYI, ***alpha***=0.21 and ***beta***=3.38; for MYI, ***alpha***=0.31 and ***beta***=3.07.

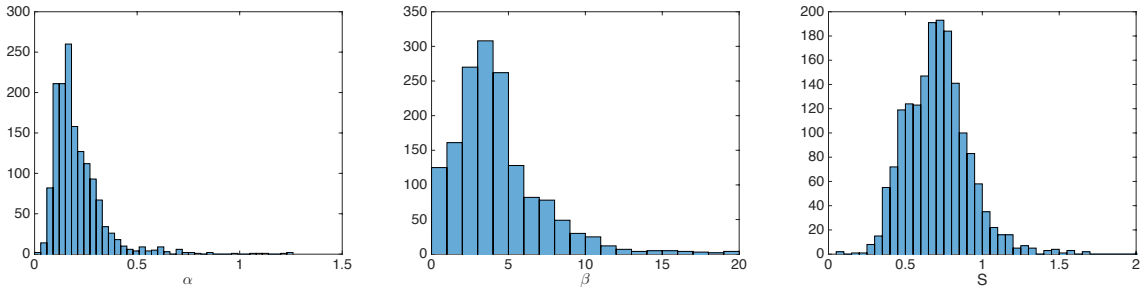

(a) ***alpha***. (b) ***beta***. (c) ***s***.

Figure 1. Distribution of alpha, beta and s for FYI. 40-meter resolution (OIB) data are used for computing the value of each parameter on the scale of 37.5 km (i.e., approximately SMOS TB resolution)

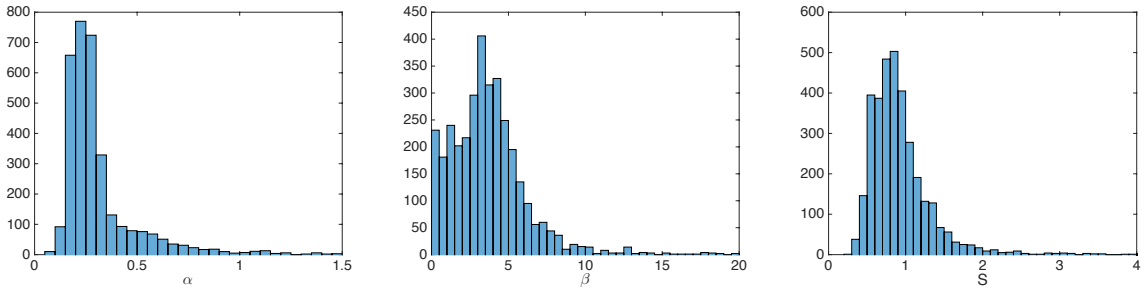

(a) ***alpha***. (b) ***beta***. (c) ***s***.

Figure 2. Distribution of alpha, beta and s for MYI. Specifications are the same as Figure 1.

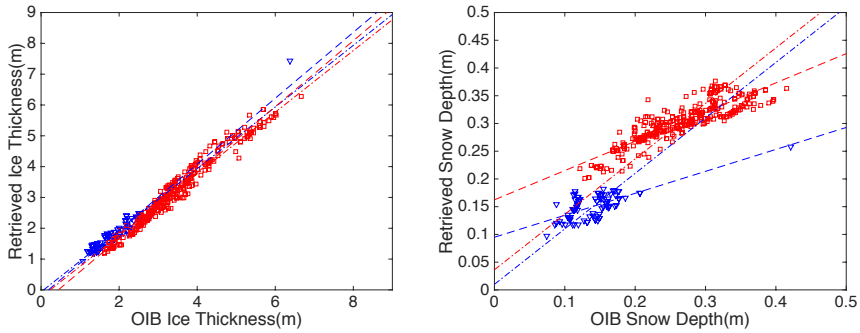

(a) ***Hi***. (b) ***Hs***.

Figure 3. Retrieval of ***Hi*** and ***Hs*** using globally fitted ***alpha*** and ***beta***.

As shown in Figure 3, with the covariability information (***alpha*** and ***beta***), indeed retrieval can be carried out. The least squares fit (dashed lines) for FYI (blue) and MYI (red) for ***Hi*** yields 0.93 and 0.96 respectively for R^2, and that for ***Hs*** yields 0.51 and 0.77. However, the least squares fit (dotted-dashed lines) for ***Hs*** on FYI (blue) yields negative R^2, and that for ***Hs*** on MYI (red) is as low as 0.15. For example, for MYI, there exists large overestimation of ***Hs*** when ***Hs*** is small, and underestimation of ***Hs*** when it is large.

Table 1. R^2 for the least-squares fit (slope=1) for the retrieval.

	Retrieval with $\boldsymbol{FB_{snow}}$, SMOS TB, and global ***s***	Retrieval with $\boldsymbol{FB_{snow}}$ and covariability (***alpha*** and ***beta***)
Hi in FYI	0.96	0.93
Hi for MYI	0.83	0.96
Hs for FYI	0.78	--
Hs for MYI	0.57	0.15

This result is in direct comparison to the retrieval carried out in the manuscript (Figure 7.c and d of the manuscript). Table 1 (above) shows the direct comparison of the R^2 for the least squares fit under the constraint of slope=1. It is shown that with the integration of SMOS TB, the quality of retrieval is improved mainly for ***Hs***. For ***Hi***, we consider the dominant factor is the value of freeboard, and the error in the retrieved ***Hs*** in Figure 3 (above) does not have big impact over the fitting for ***Hi***.

b) The retrieval as performed in this study is not very representative for an "actual" retrieval:

1. Only 50% of the available SMOS grid cells are used for the analysis, based on the criterion that "the error" (do you mean RMSE here?) between simulated and SMOS observed TB is < 1.5 K (as compared to 3.1 K for all SMOS cells). In a "real" retrieval

situation where we do not have the information from OIB (i.e. hi, hs, and surface temperature) to simulate TBs, how can we identify these cases where simulated and SMOS-observed TBs differ more?

The authors would like to clarify that: (1) the retrieval with half of the points is not an inherent limitation of the proposed method (shown below in details), (2) the RMSE of TB for all the cells is 3.1 K, while the value of 1.41 K is the RMSE of cells with better altimetry (OIB) coverage, (3) the sufficient spatial sampling of altimetry (e.g., OIB) potentially results in better retrieval results, which can be detected through other methods or data (discussed below). Since there is inherent discrepancy between the sea ice cover that generates the SMOS TB observations and that scanned by OIB (or any type of altimetry), we carry out the analysis of the TB error and its relationship to the coverage of OIB. To simplify the analysis, we use the OIB sample count (M) as the criterion for the spatial coverage of OIB. OIB campaigns include certain areas with extensive fly-over instead of a single line scan, and the effective sample count M is large for the corresponding cells. Figure 4 (below) shows the decrease of RMSE in TB (modeled v.s. SMOS) with the increase in M, analyzed over all available OIB data. For cells with larger M (i.e., over 95-percentile for M), the RMSE of TB drops from 3.1 K (for all cells) to 1.41 K, which is also mentioned in the manuscript (pg. 6, l. 5-6). Therefore, for the analysis in Section 4, we carry out retrieval for all cells with modeled TB within 1.5 K of the observed TB.

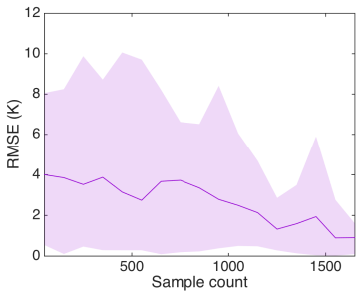

Figure 4. The relationship of RMSE of TB to OIB sample count.
For each sample count bin, the statistics of RMSE of TB are computed.
Shaded area covers the 5-th and 95-th percentile of the absolute TB error.

We have also carried out retrieval with ALL points (with SMOS TB and global value of ***s***). The verification for Hi and Hs are shown in Figure 5 (below). The quality of retrieval witnessed a slight drop when all cells are involved ($\boldsymbol{R^2}$ of 0.89 to 0.86 for ***Hi***, and 0.64 to 0.56 for ***Hs***). Still, the both parameters can be retrieved.

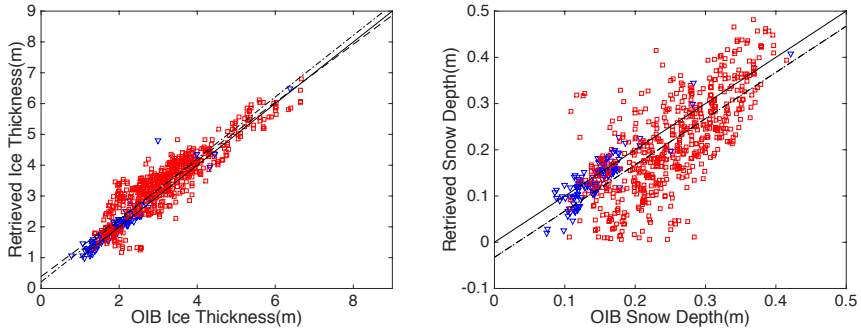

(a) ***Hi***. (b) ***Hs***.

Figure 5. Verification with all points.

As demonstrated, the lack of sufficient spatial sampling of altimetry scanning plays an important role in the forward L-band model as well as the retrieval, and it is also very important to traditional satellite altimetry. With respect to the

referee's question regarding the detection of potential TB errors, the authors consider utilizing methods and data that can support the detection of sub-cell variability of the sea ice cover (e.g., within 40km for SMOS). High-resolution remote sensing such as high-frequency radiometry (89 GHz channel from AMSR-E/2) or visible/infrared (onboard MODIS) serve as candidates. How they can be used for the study of representativeness of altimetry scans and the combined retrieval with L-band data, remains an important direction of future study.

2. In the retrieval here, TBs are simulated taking the surface temperature from OIB measurements. In a "real" retrieval situation, one would have to use other sources for surface temperature, which have different spatial and temporal resolutions; they could be (and most likely are) measured with many hours time shift! And as surface temperature has been shown to have a huge influence on L-band TB (see e.g. Maaß et al., 2013) and surface temperature can vary on short time scales, the results can be very different when using other temperature information. This is shortly mentioned at the very end of the manuscript, but it is not stressed how much this can influence the retrieval performance.

As pointed out by the referee, the surface temperature is generally not available for the retrieval. There are several third-party datasets that serve as candidates, including those based on remote sensing (such as MODIS and AMSR-E/2) and reanalysis data (e.g., ERA-Interim). Currently we are considering the retrieval on the daily basis. For example, the MODIS surface temperature field (of about 1 km of spatial resolution) on the same date of the SMOS TB is regridded to the retrieval scale of EASE grid (12.5 km), and further used for the retrieval. In a separate study, the MODIS data is adopted for the retrieval with radar altimetry (from CryoSat-2) and SMOS TB on a daily basis, and the retrieval generates good results (not shown here).
As noted by the referee, rapid change of surface temperature is present for the Arctic. However, we consider the rapid warming of the sea ice covered region is rare during winter (when altimetry is available), and mainly associated with sea ice leads, involving fast sea ice growth. As noted in Zhou et. al. (2017), the effects of open water and (refrozen) leads can be integrated in modeling of TB using third-party data (e.g., sea ice concentration and lead maps), by treating it as a small-scale variability of the sea ice cover.

3. The retrieval is done for freeboard measurements from the OIB campaign's laser altimeter. It is not discussed how the freeboard data from this altimeter compare with satellite based laser altimeters, which are given as the target for an "actual" retrieval.

The authors thank the referee for the comment on relationship with actual retrieval with satellite altimetry. The resolution of OIB is 40 m in the direction of the flight track, with the swath (across track) of about 100 m. As a comparison, for ICESat (or the to-be-launched ICESat-2) the resolution for each altimetry scan is about 70 m in diameter, with about 170 m between scans in the direction of flight track. Without considering the availability issues of laser scans (due to penetration problems caused by clouds), there exists resolution discrepancy between OIB and actual satellite measurements by ICESat.

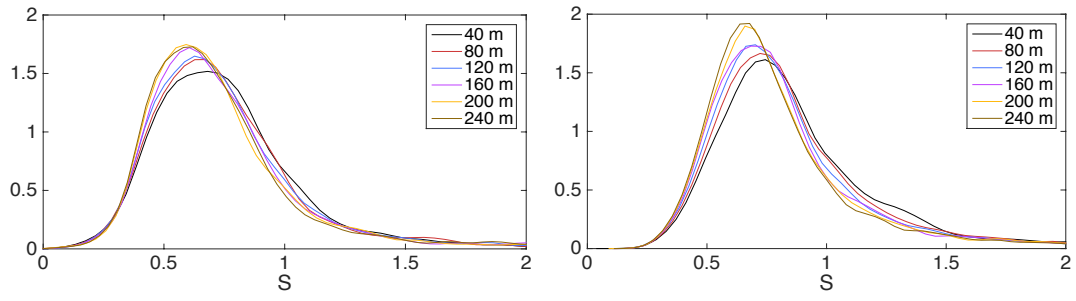

(a) FYI. (b) MYI.

Figure 6. Scaling of ***s*** derived from OIB data. PDFs of ***s*** are shown.

When working with satellite data, the characteristics of the covariability on the spatial scale of satellite altimetry has to be deduced. With respect to the covariability in the retrieval study, the issue is to compute the proper value of ***s***. We have carried out analysis by manually coarsening OIB's data to various spatial scales (by computing mean values for ***Hs*** and $\boldsymbol{FB}_{snow}$ with adjacent scans), and the results are shown in Figure 6 (above). There is a slight shift of ***s*** to smaller values for both FYI and MYI, when coarsening the OIB scans. Since ICESat(-2) features approximately 70 m spatial resolution, we intend to use the interpolated value of ***s*** between 40 m and 80 m for the potential retrieval with ICESat-2 and the concurrent satellite campaigns, such as WCOM.

c) With the current presentation of results I am not convinced that this is more than "playing around" with the relationship between ice thickness and snow depth (as observed during the OIB flights), which is taken advantage of. One would expect a relationship in that older ice is on average thicker and has had more time to accumulate snow on top, which leads to on average thicker snow on thicker ice (considering larger scales). And of course snow depth and freeboard are correlated as snow depth and ice thickness (together with snow and ice densities) determine the freeboard. Thus, I would not consider it as an "result" that you found a correlation between them. One interpretation (assuming that the densities of ice and water are relatively constant) is that the obtained R^2 value shows the fraction of the FB that is actually snow (R^2=0.53 would then mean that about 53% of the FB part consists of snow, while the rest is ice). This is also pointed out in the paper by Kwok et al. (2011), which is cited by the authors.

The authors would like to provide further proof that it is not statistics between ***Hi*** (or $\boldsymbol{FB}_{snow}$) and ***Hs*** that plays a central role in the retrieval. First, we ignore the covariability by carrying out retrieval with the mean value of $\boldsymbol{FB}_{snow}$. Specifically, for each previous retrieval problem (which involves multiple altimetry measurements and a single SMOS TB), we compute the mean of the M OIB samples of $\boldsymbol{FB}_{snow}$, denoted $\overline{\boldsymbol{FB}_{snow}}$. Then the retrieval is carried out between $\overline{\boldsymbol{FB}_{snow}}$ and TB, and the retrieved ***Hi*** and ***Hs*** are compared with the mean sea ice thickness and mean snow depth as measured by OIB (denoted $\overline{\boldsymbol{Hi}}$ and $\overline{\boldsymbol{Hs}}$). The results are shown in Figure 7 (below). This idealized retrieval scenario ignores the resolution difference between laser altimetry and L-band SMOS data. It is worth noting that no covariability is incorporated. But still good retrieval is achieved, with R^2 for ***Hi*** of 0.78 and that for ***Hs*** of 0.50.

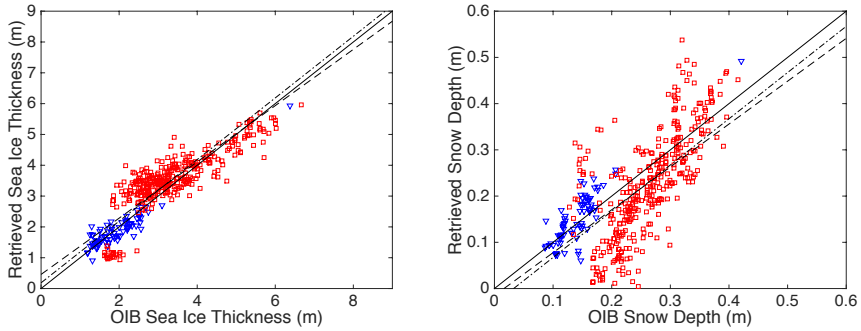

(a) ***Hi***. (b) ***Hs***.

Figure 7. Retrieval with TB and mean $\boldsymbol{FB}_{snow}$. Dashed (dotted-dashed) line in each subfigure is the least-squares line (least-squares line under the slope=1 constraint).

Second, we further compare these results with the reported results in the manuscript, which is realistic retrieval involving multiple $\boldsymbol{FB}_{snow}$ measurements from laser altimetry. With the variability (i.e., M samples), the retrieval of ***Hi*** and ***Hs*** is improved, with R^2 rising to 0.89 and 0.64, respectively (see Figure 7.c and d in the manuscript). This indicates that the altimetry sampling provides necessary information for the retrieval accuracy. It also provides further clarification of the role of the statistics during retrieval: (1) the covariability between $\boldsymbol{FB}_{snow}$ and ***Hs*** DOES play an important role for the retrievability during the realistic retrieval, which involves relatively high-resolution altimetry scans, as studied in Section 3.2 of the manuscript, and (2) the statistical information DOES NOT play a central role in the general data fusion methodology of L-band TB and laser altimetry.

Comments B:

- Acknowledgements: OIB and SMOS data are not cited correctly here, see e.g. the NSIDC's and ICDC's (University of Hamburg) conditions/suggestions of how to cite the data usage

According to referee's suggestions, the acknowledgements is revised as below: "*This work is partially supported by National Key R&D Program of China under the grant number of 2017YFA0603902 and the General Program of National Science Foundation of China under the grant number of 41575076. The authors would like to thank the editors and referees for their invaluable efforts in improving the manuscript. SMOS data is provided from Integrated Climate Data Center (ICDC), icdc.cen.uni-hamburg.de, University of Hamburg, Germany, Digital media. http://icdc.cen.uni-hamburg.de/1/daten/cryosphere/l3b-smos-tb.html. [Data Accessed: 2017/10/25]. OIB and SSM/I sea ice concentrations data are provided by NASA National Snow and Ice Data Center Distributed Active Archive Center, Boulder, Colorado USA. doi: http://dx.doi.org/10.5067/7XJ9HRV50O57. [Data Accessed: 2017/10/25]. Besides, the authors are grateful to Willmes, S. and Heinemann, G. for the provision of Arctic sea ice lead map.*".

- p. 3, L7f: "Several recent studies focus on the retrieval of snow depth over thick sea ice, based on L-band passive microwave remote sensing data from SMOS (Tian-Kunze et al., 2012)." -> I am not aware of "several" studies, they are also not given here, and the given reference (Tian-Kunze et al., 2012) is not about retrieving snow depth but (thin) ice thickness.

The authors recognize that the reference associated with snow depth retrieval is erroneous, and would like to make revision as below: "*The recent study in Maaß et al., (2013) has carried out the retrieval of snow depth over thick sea ice, by utilizing L-band passive microwave remote sensing data from SMOS*".

- p. 4, L17: As far as I know, "the OIB Level-4 product IDCSI4" that is claimed to have been used for 2012 to 2015 in this study is only available for the years 2009 to 2013... (While the IDCSI2 Quicklook data is indeed available for 2012 to 2015)

The authors recognize the reference here is incomprehensive and revised as below: "*Therein, the OIB Level-4 product IDCSI4 is adopted (Kurtz et al., 2013) for 2012-2013 and the remaining OIB data for 2014-2015 is from IDCSI2 Quicklook product, which is also available at NSIDC DAAC. Both of these two datasets are 40 m in resolution along the track's direction*".

- p. 4, L11-13: "...based on Burke et al. (1979). ... An adapted version of the model was adopted by Tian-Kunze et al. (2014) and ..." -> This is not correct. Tian-Kunze et al. (2014) use another (simpler) approach, which is originally based on a paper by Menashi et al. (1993). (also: "adapted version... was adopted" sounds strange)

The authors recognize that this is a mistake in the manuscript. The correct reference should only include Maaß et al., (2013a), which adopted the Burke's model. The whole sentence is then corrected as: "*In Maaß et al. (2013b), this model is applied to sea ice and further used for the retrieval of snow depth over thick sea ice*".

Comments C:

- p. 2, L17: "schematic view of remote sensing of sea ice" -> this seems a bit exaggerated to me, the figure mainly shows the definitions of snow and ice thickness and freeboard...

According to the suggestions of the referee, the sentence at p.2 L17 and the caption of Figure 1 are revised as follows: "*Figure 1 shows the various parameters related to satellite based laser altimetry and L-band passive radiometry for the sea ice cover*", and "*Sea ice parameters in the active and passive remote sensing of the sea ice cover, including sea ice thickness (hi), snow depth (hs) and snow freeboard (FBs)*".

- p. 2, L28-29: Not everyone knows what "its adapted version for ... FYI" is

The sentence is revised as follows: "*... climatological snow depth in Warren et al. (1999) for multi-year sea ice (MYI) and halved for first-year sea ice (FYI)*".

- p. 3, L9: Here, "near realtime" observations are compared with altimetry "which can only achieve basin coverage on the scale of about one month" -> It would be helpful to add that SMOS provides not only "near realtime" data but also "an almost daily coverage of the polar regions".

The sentence is revised as follows: "*SMOS provides full coverage of polar regions on a near real-time (daily) basis, observations with full coverage of polar regions. It has great advantage over satellite altimetry …*".

- p. 3, L13: "Despite the limited coverage..." -> strange wording/argumentation

The sentence is revised as follows: "*Although airborne remote sensing methods have limited spatial and temporal coverage, campaigns such as …*".

- p. 4, L7: "due to the limitation of satellite's orbital parameters, the inherent resolution is about 40 km" -> The resolution is determined by the antenna size, the frequency and the interferometry ("aperture synthesis") principle, not "orbital parameters".

The authors recognize the correction by the referee, and the sentence is revised as: "*However, due to the limitation of satellite's antenna size, the effective resolution of L-band radiometer onboard SMOS is about 40 km.*"

- p. 4, L25-26: "we consider OIB measurements in the adjacent 3x3 cells ... of equal contribution" -> Maybe mention at least that this is an approximation (the contributions are actually not equal, see the SMOS "antenna gain function")

According to the referee's suggestion to clarify the description, the authors have made two modifications. First, a sentence is added in the SMOS data description in Section 2.1: "*The gridded SMOS TB data field is generated from multiple snapshots within a day, with each snapshot involving multiple incident angles and spatially varying gain*". Second, the sentence mentioned by the referee is revised as "*However, due to the inherent resolution of SMOS is about 40 km and the daily gridded field is used in this study, we approximate the correspondence of OIB and SMOS TB by considering OIB measurements in the adjacent 3x3 cells (the red segment in Figure2) of equal contribution to the SMOS TB at the central cell (the one bounded by thick blue lines in Figure 2)*".

- p. 4, L30-31: "However, for certain segments of the OIB tracks, there exists extensive scanning which corresponds to a much larger value of M." -> I think it would be better and more precise to state the range of encountered M values (e.g. giving minimum, maximum and mean).

Figure 8 (below) shows the distribution of *M* for all available OIB data. The mean value of *M* is about 700. The referee is also kindly directed to Figure 4 (above) for the relationship between *M* and the RMSE of TB. Revision to the manuscript is also made to reflect the statistics of *M*.

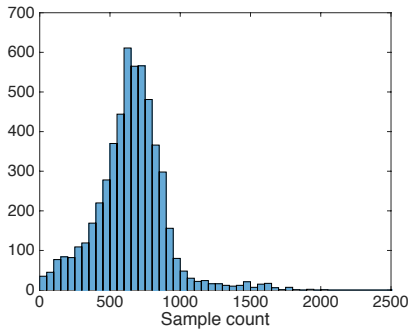

Figure 8. Distribution of OIB sample count (*M*).

- p. 5, L3-5: "The purpose of these treatments is to rule out the factors that may compromise the quality of the OIB samples and allow focus on the discussion of the retrieval algorithm." -> However, these conditions that were excluded here do not only influence the OIB data quality but will probably also make a potential retrieval with SMOS data more difficult and should be discussed somewhere.

The authors would like to point out that, indeed open water and (refrozen) leads can have profound effect on the overall TB, indicated by Kaleschke et al. (2010) and Tian-Kunze et al. (2014), and also studied in Zhou et al. (2017). Specifically, in Zhou et al. (2017), their effect is integrated into the radiation model by considering them (i.e., open water, leads) as a sub-scale mixture of the sea ice cover. Besides, a thermodynamic model for the diagnosis of ice thickness within the leads is adopted. For the basin-scale retrieval, these factors definitely should be considered, by using third-party data as indicators. But for the current study, we focus on the retrieval methods, therefore their effects are not considered. Outlook to how their effects should be accounted for is now included in Section 5 in the revised version of the manuscript.

- p. 5, L16: Reference to used radiation model should be given already here.

From the given reference it is not clear how the authors of that paper have "reformulated the model to include multiple layers for sea ice and snow" (Zhou et al, 2017). If several ice layers are used in the model, the higher order reflection terms should be considered. I did not find a statement on this...

Following the suggestion of the referee, the authors add the reference to Zhou et al. (2017) to this sentence. The work for the study of radiation model is now currently available online (see Zhou et al. (2017)). The non-coherent model from Burke et al. (1979) and its adaptation to sea ice in Maaß et al. (2013a) is the basis for the study in Zhou et al. (2017). Since much higher overestimation of TB was witnessed for MYI, in Zhou et al. (2017) the drainage of salinity in the top part of the MYI is accounted for, by using a multi-layer formulation of the model. We provide a model description document as a supplement to the revised manuscript.
The original model in Burke et al. (1979) ignores the high-order terms for reflection (beyond 2nd order). As reported in Maaß et al. (2013b), there exists different behavior of the multi-layer of Burke's model and the multi-layer coherent Ulaby model. However, two aspects that are relevant to the current study: (1) as compared with the drainage of top-layer salinity, the multi-layer formulation induces a smaller change as compared with the single-layer formulation (adopted by Maaß et al. (2013a)), and for MYI, the integration of salinity profile resulted in a much better fit of modeled TB to SMOS observation, as shown in Zhou et al. (2017); and (2) as shown in Figure 3.c of the manuscript, the potential of retrieval lies in that the retrieval is carried out over constant freeboard lines, and even if TB saturates (beyond 3 m for ***Hi***) there still exists good sensitivity for retrieval.

- p. 7, Eq. 3: Maybe better to use "arctan(...)" because tan^-1(...) could also be interpreted as 1/tan(...)

Corrected according to the referee's suggestion. All other cases including "*tan^-1*" in the manuscript are corrected to "*arctan*" as well, in order to avoid misinterpretation and ensure consistency.

- p. 8, L5 - p. 9, L19: First you write about "scanning of alpha" without explaining it at all, then you present the results shown in Fig. 5. Then you explain the "scanning of alpha" procedure and finally refer to Tab. 2. This is very confusing. The scanning of alpha should be explained first. It would also be very interesting to see what values alpha takes in this procedure. Are they similar for the individual retrievals? Are they spread over a large range? Do the results shown in Fig. 5 and Tab. 2 belong to the same analysis?

According to the suggestions of the referee, we have made revisions to the manuscript: (1) first we include the description of ***alpha*** and the scanning of it in Section 3.2 (on p. 9), (2) in Section 4, the scanning of ***alpha*** is introduced in the retrieval process in more clear way. Figure 1 and 2 of this response document also provide the statistics of ***alpha***. As shown, with OIB data, there exists a large range of possible values for ***alpha***, which is also indicated by the retrieval process (which generates the value of ***alpha*** as well). In Figure 9 (below), for the typical distribution of $\boldsymbol{FB_{snow}}$ for both FYI and MYI (subfigure a), the scanning of ***alpha*** and the resulting mean ***Hs*** is shown (subfigure b). Since the value of ***s*** is smaller than 1, there exists no inundation, which is consistent to the rarity of such events in the Arctic. Besides, indeed, Figure 5 and Table 2 of the manuscript belong to the same analysis.

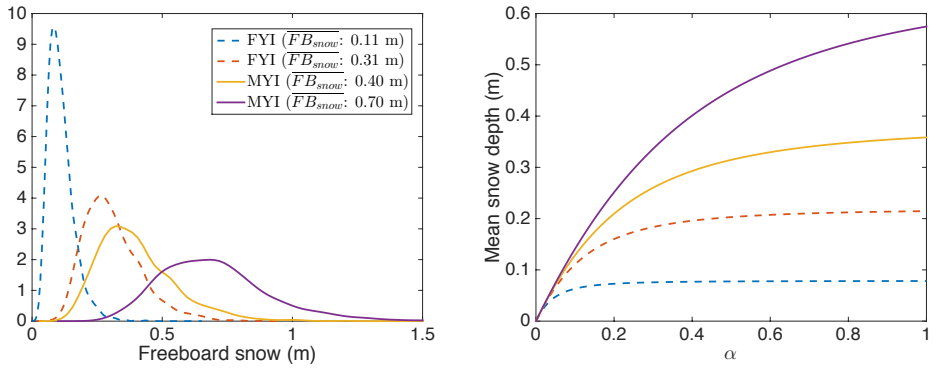

(a) $\boldsymbol{FB_{snow}}$ distribution. (b) Mean ***Hs***.

Figure 9. Scanning of parameter α and the corresponding mean snow depth (***Hs***).

- p. 10, L3-6: "There is minor increase in quality (0.91 versus 0.89 and 0.65 versus 0.637) and a relatively large gap to the "ideal" case. This indicates that the uncertainty (or error) in TB and radiation models plays an important role in affecting the quality of the retrieval.

The uncertainty of TB may arise from that of the radiation model, as well as the mismatch between the altimetry and passive microwave remote sensing" I think the very similar results for simulated and SMOS TBs cannot lead to these conclusions about the radiation model or the TB measurements! Even if (theoretically) the radiation model gave completely unrealistic TB values: If you do the hs/hi-retrieval by comparing this radiation model's TBs (for different hs,hi values) with this same radiation model's "true" TB (for the "true" hs,hi values), the difference in retrieved and "true" hs,hi will originate from other assumptions used in the retrieval (here: assumption of Eq. 3, choice of s-value, choice of thresholds, ...) or from the ill-posedness of the problem (TB ambiguities in the model, which can also exist in reality) but not the quality of the model to represent the "real world"/SMOS (because you are comparing it with its own output! You are within its "ideal model world"). In contrast, an existing difference between using SMOS and simulated TBs may contain information on the radiation model's performance to simulate SMOS TBs (and also on the effect of the spatial mismatch between altimeter and satellite measurements).

As far as I can see, the difference between using global and local s values tells you something about how good the global s value approach is. Here (with the results for simulated and SMOS TBs being very similar), THIS (=using different s values) is where the "relatively large gap to the 'ideal' case" seems to come from!

After careful re-check of the manuscript and the results, the authors have discovered a mistake in the manuscript, and would like to sincerely apologize for the error and potentially misleading the referee. The retrieval result with R^2 of 0.91 for ***Hi*** and 0.65 for ***Hs*** is attained with the local value of ***s*** and SMOS TB, and NOT with the global value of ***s*** and the modeled TB. In the manuscript (pg. 10, l. 1-3), the correct sentence should be: "*Furthermore, if the retrieval is based on: (1) observed TB from SMOS, and (2) the locally fitted value of* ***s****, the* R^2 *values for the fitting are 0.91 and 0.65 for sea ice thickness and snow depth respectively, with virtually no change in the fitting lines (not shown)*". For the sake of completeness, we have also carried out retrieval with the other combination of modeled TB and global value of ***s***, and the R^2 values are 0.96 and 0.84 for ***Hi*** and ***Hs***, respectively. These values are very close to the "ideal" retrieval case (which involves modeled TB and the local value of ***s***). All the results for fitting (for all 4 combinations) are shown in Figure 10 (below). These results indicate that the difference between modeled and observed TB is indeed a major source of the retrieval error, especially for ***Hs***, which is a "correctly" stated sentence in the manuscript (i.e., the sentence the referee mentioned).

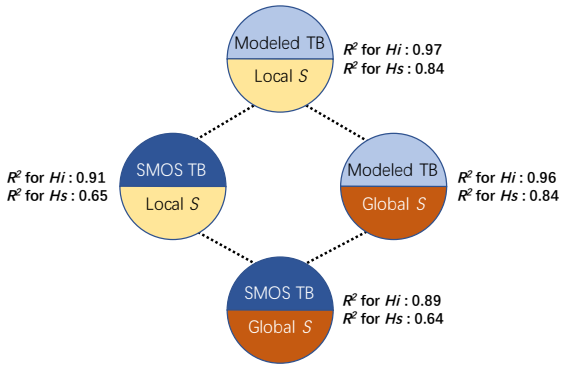

Figure 10. Comparison of different configurations in retrieval. Each circle represents the retrieval with the specific TB and the value of ***s***. The bottom circle represents the realistic retrieval scenario, and the top one represents the "ideal" scenario. The fitting to observations (R^2) for both ***Hi*** and ***Hs*** are shown accordingly.

The authors would like to emphasize again that the even if with the mean freeboard and TB, both ***Hi*** and ***Hs*** can be retrieved (shown in Figure 7 above). However, when the information of altimetry samples is incorporated, better retrieval can be achieved for both ***Hi*** and ***Hs***. For the retrieval which accounts for the resolution difference between L-band TB and laser altimetry, covariability plays an important role in the retrievability.

- Fig. 5 would benefit from a legend and/or annotations of some of the lines, it is hard to remember from the figure caption what each of the 7 lines represents...

Legends are added to each of the subfigures of Figure 5 for better readability. The updated figure is available in the revised manuscript. They are also reproduced below in Figure 11.

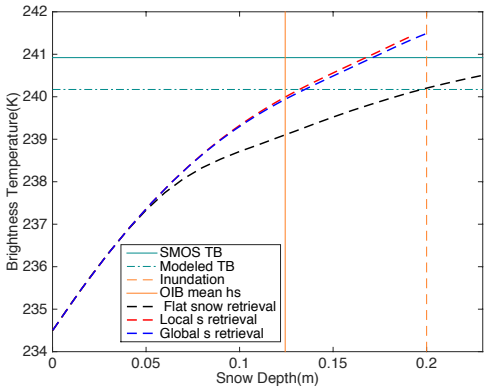

(a) Scenario I

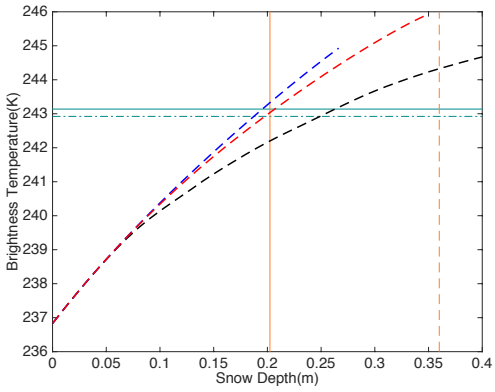

(b) Scenario II

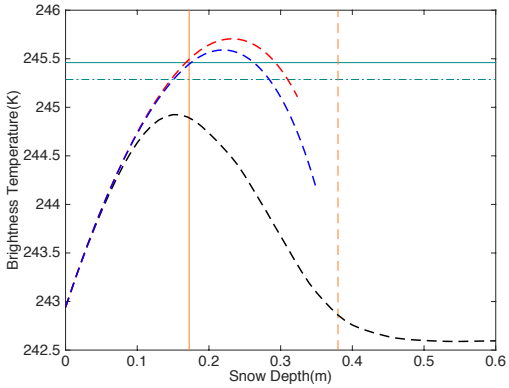

(c) Scenario III

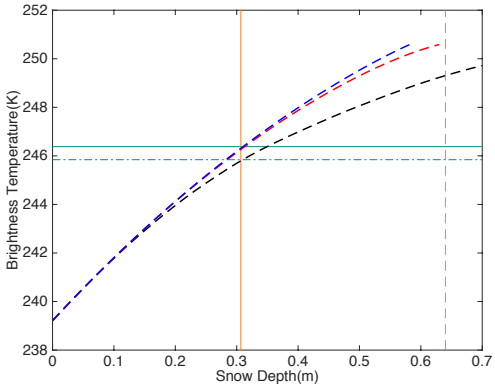

(d) Scenario IV

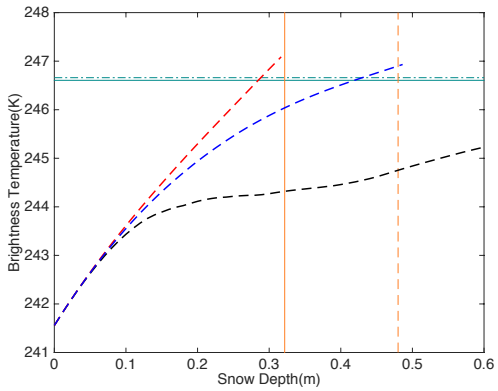

(e) Scenario V

Figure 11. Updated Figure 5 of the manuscript.

Comments D (not a complete list!):

- Usage of "etc" is not very precise, for example on p. 2, L5 & p. 2, L20 & p. 4, L11 & p. 5, L34

The authors have made revisions to the manuscript for corrections and more precise use of “etc”, including those pointed out by the referee. Unnecessary uses of “etc” are deleted.

- p. 2, L5-6: "there is rapid" -> "there has been rapid"

Corrected.

- p. 2, L24: "hence limited spatial coverage" -> not a complete sentence

Corrected as: "*..., so they are limited in terms of spatial coverage*".

- p. 3, L6: "researches...obtain snow depth" -> strange wording

This sentence is revised by segmenting into three parts: "*The retrieval of snow depth with passive microwave satellite remote sensing has been carried out in various studies. In Comiso et al., (2003), multi-band data from AMSR-E are utilized, but only for FYI. Maaß et al., (2013b) explored the retrieval of snow depth over thick sea ice with L-band data from SMOS*".

- p. 3, L10: "requires the prerequisite" -> either "requires" or "prerequisite"

Corrected as follows: "*However, the sea ice thickness is required for the retrieval*".

- p. 3, L25: "achieves successfully retrieval" is not a correct expression

This sentence is revised as follows: "*..., we demonstrate that the proposed algorithm can simultaneously retrieve both sea ice thickness and snow depth, ...*".

- p. 3, L26: "correspond" -> "corresponds"

Corrected.

- p. 4, L20: "Temporally, the date of each OIB campaign is located, and the SMOS TB data from the specific date is attained for the combined retrieval." -> An example for a case where the readability could be improved. This sounds like a complicated way of saying something like: "OIB and SMOS data from the same day are taken."

Corrected as indicated by the referee as follows: "*OIB and SMOS data from the same day are taken.*"

- p. 4, L23-24: "due to the inherent resolution of SMOS data is about 40km, therefore..." is not a correct expression

The sentence is corrected as follows: "*However, since the inherent resolution of SMOS data is about 40 km, even if the SMOS data product is provided on the 12.5 km resolution (small blue cells in Figure 2), we consider OIB measurements in the ...*"

- p. 4, L26: "the 9 cells covers" -> "the 9 cells cover"

Corrected.

- p. 4, L28: "the total area the contributes" -> "the total area that contributes"

Corrected.

- p. 6, L28 - p. 7, L7: This part is hard to understand...

The authors would like to explain that: the purpose of this paragraph is to introduce the protocol in the covariability analysis. For clarity, the whole paragraph is revised as follows:

"*For the covariability between* $\boldsymbol{FB_{snow}}$ *and* ***Hs****, we choose the native resolution of the OIB product (40 m) as the spatial scale for analysis. Each TB corresponds to multiple (M) OIB samples, with each sample containing the measurement for both* $\boldsymbol{FB_{snow}}$ *and* ***Hs****. We divide these samples into* $\boldsymbol{FB_{snow}}$ *bins, with each bin covering 5 cm. In total there are 30 bins, covering the range of 0 to 1.5 m. For samples in each bin, we compute the percentiles and the mean value of* ***Hs****. Figure 4.a shows the mean* ***Hs*** *and the +/-1 standard deviation range and their relationship with* $\boldsymbol{FB_{snow}}$*, for 4 representative TB points. Furthermore, we carry out least squares fitting (weighted according to sample count in each bin) between mean* ***Hs*** *and* $\boldsymbol{FB_{snow}}$*. Among all available TB and OIB data, there exist statistically significant positive correlation between* ***Hs*** *and* $\boldsymbol{FB_{snow}}$ *for over 90% of all points. The values of* R^2 *are in the range of 0.06 and 0.89 (95% percentile), with the mean value of* R^2 *of 0.53. This indicates that there exists consistent covariability between snow depth and snow freeboard across Arctic sea ice cover*."

- p. 8, L1-2: "For hs > 0, there will be inundation due to: FB< hs." -> Do you mean: "For hs> 0, there will be inundation for values hs>FB."?

The referee's guess is right. For the sake of clarity, this sentence is revised as: "*For any sample of* $\boldsymbol{FB_{snow}}$*, if the value of freeboard is smaller than the current value of* ***hs****, in order to avoid inundation, the snow depth for this sample is assumed to be the same as* $\boldsymbol{FB_{snow}}$".

The authors would like to express sincere thanks to the referee for the insightful comments and invaluable suggestions to the manuscript. Revisions to the manuscript are made according to the suggestions. We hope that through the reply and the revised manuscript, the idea and results are now better conveyed to the referee. We would also like to answer any further questions and comments from the referee.

References:

Kaleschke L, Maaß N, Haas C, et al. A sea-ice thickness retrieval model for 1.4 GHz radiometry and application to airborne measurements over low salinity sea-ice[J]. The Cryosphere, 2010, 4(4): 583-592.

Maaß, N., Kaleschke, L., Tian-Kunze, X., and Drusch, M., 2013a: Snow thickness retrieval over thick Arctic sea ice using SMOS satellite data, The Cryosphere, 7, 1971–1989, doi:10.5194/tc-7-1971-2013, www.the-cryosphere.net/7/1971/2013/.

Maaß N, Kaleschke L, Stammer D. Remote sensing of sea ice thickness using SMOS data[D]. University of Hamburg Hamburg, 2013b.

Tian-Kunze, X., Kaleschke, L., Maaß, N., Serra, M. M. N., Drusch, M., and Krumpen, T.: SMOS-derived thin sea ice thickness: algorithm baseline, product specifications and initial verification, The Cryosphere, 8, 997–1018, doi:10.5194/tc-8-997-2014, www.the-cryosphere.net/8/997/2014/, 2014.

Zhou L, Xu S, Liu J, et al. Improving L-band radiation model and representation of small-scale variability to simulate brightness temperature of sea ice[J]. International Journal of Remote Sensing, 2017, 38(23): 7070-7084.

On the Retrieval of Sea Ice Thickness and Snow Depth using Concurrent Laser Altimetry and L-Band Remote Sensing Data

Lu Zhou[1], Shiming Xu[1], Jiping Liu[2], and Bin Wang[1,3]

[1]Ministry of Education Key Laboratory for Earth System Modeling, Department of Earth System Science, Tsinghua University, Beijing, China
[2]Department of Atmospheric and Environmental Sciences, University at Albany, State University of New York, Albany, NY, USA
[3]State Key Laboratory of Numerical Modeling for Atmospheric Sciences and Geophysical Fluid Dynamics (LASG), Institute of Atmospheric Physics, Chinese Academy of Sciences, Beijing, China

Correspondence to: Shiming Xu (xusm@tsinghua.edu.cn)

Abstract. The accurate knowledge of sea ice parameters, including sea ice thickness and snow depth over the sea ice cover, are key to both climate studies and data assimilation in operational forecasts. Large-scale active and passive remote sensing is the basis for the estimation of these parameters. In traditional altimetry or the retrieval of snow depth with passive microwave sensing, although the sea ice thickness and the snow depth are closely related, the retrieval of one parameter is usually carried out under assumptions over the other. For example, climatological snow depth data or as derived from reanalyses contain large or unconstrained uncertainty, which result in large uncertainty in the derived sea ice thickness and volume. In this study, we explore the potential of combined retrieval of both sea ice thickness and snow depth using the concurrent active altimetry and passive microwave remote sensing of the sea ice cover. Specifically, laser altimetry and L-band passive remote sensing data are combined using two forward models: the L-band radiation model and the isostatic relationship based on buoyancy model. Since the laser altimetry usually features much higher spatial resolution than L-band data from Soil Moisture Ocean Salinity (SMOS) satellite, there is potentially covariability between the observed snow freeboard by altimetry and the retrieval target of snow depth on the spatial scale of altimetry samples. Statistically significant correlation is discovered based on high-resolution observations from Operation IceBridge (OIB), and with a nonlinear fitting the covariability is incorporated in the retrieval algorithm. By using fitting parameters derived from large-scale surveys, the retrievability is greatly improved, as compared with the retrieval that assumes flat snow cover (i.e., no covariability). Verifications with OIB data show good match between the observed and the retrieved parameters, including both sea ice thickness and snow depth. With detailed analysis, we show that the error of the retrieval mainly arises from the difference between the modeled and the observed (SMOS) L-band brightness temperature (TB). The narrow swath and the limited coverage of the sea ice cover by altimetry is the potential source of error associated with the modeling of L-band TB and retrieval. The proposed retrieval algorithm (or methodology) can be applied to the basin-scale retrieval of sea ice thickness and snow depth, using concurrent passive remote sensing and active laser altimetry based on satellites such as ICESat-2 and WCOM.

1 Introduction

Sea ice is an important factor in the global climate system, playing key roles in modulating atmosphere and ocean interaction in the polar regions, the radiation budget through albedo effects, the ocean circulation through salinity and freshwater distribution (Screen and Simmonds, 2010; McPhee et al., 2009; Kurtz et al., 2011; Perovich et al., 2011). In the last decades, there has been rapid shrinkage of Arctic sea ice cover (Rothrock et al., 1999; Comiso et al., 2008; Stroeve et al., 2012; Laxon et al., 2013; Stocker et al., 2013), particularly in summer. In addition, the Arctic sea ice is also experiencing dramatic thinning in recent years (Kwok et al., 2009; Laxon et al., 2013), with the transition to overall younger sea ice age. Besides, the snow as accumulated over the sea ice cover also plays important roles due to its higher albedo as compared with sea ice, as well as thermal insulation which further hinders atmosphere-ocean interaction. With respect to changes in the sea ice cover, there is also significant decrease of the snow depth over the sea ice cover in the Arctic (Webster et al., 2014) which bears great deviation from climatology (Warren et al., 1999), indicating changes in the hydrological cycles such as late accumulation due to late freeze onset. The accurate knowledge of the sea ice cover and the snow over the sea ice, is key to the understanding of related scientific questions in climate change, as well as operational usage such as seasonal forecast.

The basin-scale observation of the sea ice cover mainly relies on satellite based remote sensing. Among the various sea ice parameters based on satellite retrieval, the most established is the sea ice concentration (or coverage). Figure 1 shows the various parameters related to satellite based laser altimetry and (L-band) passive radiometry for the sea ice cover. Passive microwave remote sensing of both Arctic and Antarctic is the basis of the retrieval of sea ice extent, with near realtime coverage since about 1979 based on satellite campaigns such as Scanning Multichannel Microwave Radiometer (SMMR), the Special Sensor Microwave/Imager (SSM/I) (Cavalieri et al., 1999), AMSR-E (Comiso et al., 2003), AMSR2 (Toudal Pedersen et al., 2017). However, the sea ice thickness is generally not retrievable through passive remote sensing techniques due to the saturation of radiative properties especially for high frequency ranges such as SMMR or SSM/I. In situ measurements of ice thickness through moored upward-looking sonar instruments and electromagnetic induction sounders mounted on sledges, ships, or helicopters/airplanes can provide sea ice thickness at specific locations or cross sections (Stroeve et al., 2014), so they are limited in terms of spatial coverage. Active remote sensing of satellite altimetry measures the overall height of the sea surface, serving as the major approach for the thickness retrieval of the sea ice. For radar altimetry, it is usually assumed that the radar signals penetrate the snow cover, and the main reflectance plane is the sea ice-snow interface (Laxon et al., 2003, 2013). Therefore in radar altimetry, the sea ice freeboard is measured. The sea ice thickness can be retrieved under certain estimation of the snow loading, such as climatological snow depth data in Warren et al. (1999) for multi-year sea ice (MYI) and halved for the first-year sea ice (FYI). Besides, for laser altimetry as in ICESat (Kwok and Cunningham, 2008; Kwok et al., 2009), the main reflectance surface is the snow-air interface, and the directly retrieved value is actually the snow (or total) freeboard. The snow loading is also required for the conversion of the snow freeboard to the sea ice thickness. As analyzed in Tilling et al.

(2015) and Zygmuntowska et al. (2014), the uncertainty in snow depth is the most important contributor to that of the sea ice thickness and volume.

The major reason of the uncertainty in snow depth and the loading on the sea ice cover is the lack of stable product for snow depth over the sea ice with good temporal and spatial coverage. The snow data as used in ICESat (Kwok and Cunningham, 2008) is derived from reanalysis data and satellite retrieved sea ice motion, while the climatological snow depth data in Warren et al. (1999) as used by CryoSat-2 (Laxon et al., 2013) contains large uncertainty due to interpolation and interannual variability, and may not be adequate for the present day under the context of climate change (Kwok et al., 2011; Webster et al., 2014). The retrieval of snow depth with passive microwave satellite remote sensing has been carried out in various studies. In Comiso et al. (2003), multi-band data from AMSR-E are utilized, but only for FYI. Maaß et al. (2013b) explored the retrieval of snow depth over thick sea ice with L-band data from SMOS. SMOS provides full coverage of polar regions on a near real-time (daily) basis. It has great advantage over satellite altimetry which can only achieve basin coverage on the scale of about one month. However, the sea ice thickness is required for the retrieval. Besides, with the better penetration of L-band signal in the sea ice cover, it is also demonstrated that there is retrievability of thin sea ice thickness with L-band data, as in Kaleschke et al. (2010) and Tian-Kunze et al. (2014). Although airborne remote sensing methods have limited spatial and temporal coverage, campaigns such as NASA's Operation IceBridge (OIB) carry out high-resolution scanning of the sea ice cover (Kwok et al., 2011; Kurtz and Farrell, 2011; Kurtz et al., 2013; Brucker and Markus, 2013), and provide invaluable data that are organized into flight-track based segments of the sea ice cover. The data can be adopted for the analysis of the status and variability of the sea ice cover at fine scale, as well as basin-scale studies as in Webster et al. (2014).

In this article, we propose a new algorithm that achieves simultaneous retrieval of both sea ice thickness and snow depth, based on two observations: the L-band passive microwave remote sensing and the laser altimetry that measures total freeboard. The potential of retrieval of these parameters lies in that both observations (freeboard and L-band radiative properties) are decided by these sea ice parameters. Specifically, we use OIB data (sea ice thickness, snow depth and snow freeboard) and concurrent SMOS L-band brightness temperature (TB) to simulate the simultaneous retrieval. It is found that the covariability of snow depth and freeboard at the local scale can greatly affect the well-posedness of the retrieval problem, and it is crucially important to include such covariability in the retrieval algorithm. Based on both realistic retrieval scenarios and large-scale retrieval with OIB and SMOS data, we demonstrate that the proposed algorithm can simultaneously retrieve both sea ice thickness and snow depth, and the error in the retrieved parameters mainly arises from the discrepancy between the sea ice area that corresponds to the SMOS measurement and that scanned by OIB. In Section 2 we first introduce the data, the models and the protocol of combined retrieval. Detailed statistics of snow depth and the effects of covariability on retrievability is covered in Section 3. Based on the statistics, we propose the retrieval algorithm and carry out evaluation and analysis in Section 4. Section 5 summarizes the article and provides discussion of related topics and future work.

2 Data and Models

2.1 Data

In order to construct and evaluate the retrieval algorithm, we mainly utilize two datasets, SMOS and OIB. SMOS measures the microwave radiation emitted from the Earth's surface in L-band (1.4GHz). In this article, we adopt the L3B TB product from SMOS. The daily gridded SMOS TB data field is generated from multiple snapshots within a day, with each snapshot involving multiple incident angles (ranging from 0 ° to 40 °) and spatially varying gain. The data is provided on the Equal-Area Scalable Earth (EASE) grid with a grid resolution of 12.5 km. However, due to the limitation of the satellite's antenna size, the effective resolution of L-band radiometer onboard SMOS is about 40 km

High-resolution airborne remote sensing of sea ice parameters are available from OIB missions, starting in 2009 and covering western Arctic during winter months (mainly around March). This paper utilizes OIB measurements from 2012 to 2015, during which the measurements include surface temperature of the sea ice cover. The product is organized into tracks, and includes along-track measurements of total freeboard, surface temperature, snow depth. Due to the nature of the airborne measurements, the observations are limited to a narrow swath on the order of 100 m. Snow freeboard products are produced from Airborne Topographic Mapper (ATM) laser altimeter (Krabill and B., 2009). Sea ice thickness is retrieved from snow freeboard and snow depth, which is measured by the University of Kansas' snow radar (Leuschen, 2014). Surface temperature is determined from the IceBridge KT-19 infrared radiation pyrometer data set (Shetter et al., 2010). There is also accompanying sea ice type information, which is from Norwegian Meteorology Service OSI SAF system (Aaboe et al., 2016). Therein, the OIB Level-4 product IDCSI4 is adopted (Kurtz et al., 2013) for 2012-2013 and the remaining OIB data for 2014-2015 is from IDCSI2 Quicklook product, which is also available at NSIDC DAAC. Both of these two datasets are 40 m in resolution along the track's direction.

2.2 Data usage protocols

Due to the difference between OIB and SMOS data in both temporal and spatial coverage, we outline the following protocols of using the two data sets. OIB and SMOS data from the same day are taken. Spatially, for each OIB flight track, we locate all the EASE grids that contain OIB measurements. Figure 2 shows a typical case. Since OIB measurements are of a small swath, we consider the OIB data (of 40 m resolution) are samples of the underlying sea ice cover that contributes to a single SMOS TB measurement. However, due to the inherent resolution of SMOS is about 40 km and the daily gridded field is used in this study, we approximate the correspondence of OIB and SMOS TB by considering OIB measurements in the adjacent 3×3 cells (the red segment in Figure 2) of equal contribution to the SMOS TB at the central cell (the one bounded by thick blue lines in Figure 2). In total, the 9 cells cover an area of about 37.5 km × 37.5 km, which is coherent with the physical resolution of SMOS data.

It is worth noting that the area as covered by a single scan of the OIB track consists of less than 5 % of the total area that contributes to the SMOS TB. Therefore, we only treat the OIB data as samples of the underlying sea ice cover. The OIB sample count (denoted M) ranges from several hundreds to over 1000. The mean value of M is about 700, but there exists certain

areas with extensive scanning, which corresponds to a large value of M. Figure S2 shows the distribution of M for all available OIB data.

In order to exclude the potential effect of insufficient sampling or the inhomogeneity of the sea ice cover, we further exclude the following data for the analysis and evaluation. First, if an area is under-sampled by OIB (M <100), it is not considered for further analysis. Second, we exclude the cases in which a single SMOS TB corresponds to OIB samples with different sea ice types (i.e., mixed MYI and FYI). Third, we also exclude the cases involving sea ice leads as detected by the sea ice lead map in Willmes and Heinemann (2015a) or sea ice concentration lower than 1 according to Cavalieri et al. (1996). The purpose of these treatments is to rule out the factors that may compromise the quality of the OIB samples and allow focus on the discussion of the retrieval algorithm.

The snow freeboard as measured by OIB and the SMOS TB are used for the retrieval. The mean snow depth and mean sea ice thickness as measured by OIB are used for verification of the retrieval. Besides, since we assume the underlying sea ice cover as homogeneous within the retrieval scale (within 9 cells) and treat OIB measurements as samples to it, we also use the M measurements of snow depth to study the statistics of the snow depth and its covariability with snow freeboard.

2.3 L-band radiation model

The L-band (1.4 GHz) radiative property of the sea ice cover is characterized through numerical modeling based on Burke et al. (1979). The model was originally designed for the modeling of radiative transfer of the X- and L-band soil moisture. In Maaß et al. (2013b), this model is applied to sea ice and further used for the retrieval of snow depth over thick sea ice. These works, a simple 1-layer formulation is used for both the sea ice and the snow cover over it. In order to better characterize the radiative properties of the sea ice, in this article we use a multi-layer formulation of the model with sea-ice type dependent vertical salinity and temperature profile (Zhou et al., 2017). The temperature profile in the vertical direction is linear in either the snow cover and the sea ice, assuming homogeneous thermal conductivity within the snow or the sea ice. Therefore the temperature in each sea ice or snow layer can be fully decided given the parameters of thermal conductivity, the ice bottom temperature (assumed to be -1.8 $^{\circ}C$), and the snow surface temperature. The salinity profile of FYI differs from that of MYI. For FYI, the salinity of all layers of the sea ice all equals the bulk salinity, which decreases with the sea ice thickness. For MYI, a surface-drained profile is adopted to reflect the effect of summer melt and flushing. Figure 3.a shows the sea ice salinity profiles under the different sea ice types or thickness. The dielectric properties, the emissivity of the layers and the overall radiative properties of the sea ice cover is modeled, following Kaleschke et al. (2010) and Maaß et al. (2013a). The convergence of the modeled TB with respect to the layer count is witnessed, which is consistent with the study in Maaß et al. (2013a). In Zhou et al. (2017), it is demonstrated that the multi-layer treatment and the salinity profile MYI yields good fit between the simulated TB and SMOS TB. Part 1 of the supplementary material provides introduction to the details of the model, including the verification with OIB and SMOS data. Figure 3.c shows the modeled TB under typical sea ice parameters for MYI under typical winter Arctic conditions (surface temperature of -30 $^{\circ}C$). The green contour lines are constant FB_s lines. With the thickening of sea ice cover, the value of TB increases and saturates when hi is large enough (larger than 2.5 m). The value of TB is not monotonic with respect to FB_s, and for certain value combinations of snow freeboard and TB, two

solutions are possible. This results in the potential problem of ill-posedness for the retrieval with realistic observational data, as is discussed in Section 3.2.

In order to match the protocol of the SMOS TB data product, we also simulate the mean of horizontal and vertical polarization TB among 0 ° to 40 °. We consider the correspondence between a single SMOS TB value and the arithmetic mean of all the M TB values simulated by the radiation model using the M corresponding OIB samples (each with sea ice thickness, snow depth, surface temperature and sea ice type). Figure 3.b shows the comparison of modeled TB and SMOS TB, by using all available data. The least squares (LSQ) fit line (dashed line) and the LSQ fit line with the constraint that the slope be 1 (dotted line) are shown. The root mean square error (RMSE) in modeled TB as compared with SMOS data is about 3.1 K. The R^2 value for the second fit is 0.54 with an intercept of $-1.637K$, which is treated as a model bias and canceled in further studies. As noted in Section 2.2, there is potentially insufficient sampling of OIB data, so we further consider areas with more extensive OIB sampling. Specifically, cells with large values of sample count M (over 95 percentile) are considered to be more thoroughly scanned spatially, and the RMSE of TB for these cells drops to 1.41 K. Figure S3 shows the relationship between RMSE of TB to the value of M, which demonstrates that the lack of sufficient spatial coverage is an important source for the difference between the modeled TB and the SMOS observation. Based on the aforementioned RMSE of 1.41 K for well-surveyed regions, we only consider the retrieval for cells with an TB error within 1.5 K for further studies. In all 412 TB cells are available, containing 35 OIB tracks and 321'168 OIB measurements. They account for about 50% of all available TB cells. We consider this is a limitation of combined usage of OIB and SMOS data, and the retrieval with actual satellite laser altimetry and L-band TB can be free from this limitation through better altimetric scanning and wider swath as compared with OIB.

2.4 Isostatic equilibrium model

Apart from the L-band radiation model, the other model as used by the retrieval is the equilibrium model based on the buoyancy relationship. Under certain assumptions of the sea ice density (denoted ρ_{ice}), sea water density (denoted ρ_{water}) and snow density (denoted ρ_{snow}) and the equilibrium state, the sea ice thickness, snow depth and snow freeboard FB_s are constrained according to Equation 1. And the sea ice thickness can be derived given the snow depth, according to Equation 2. This model is widely applied for both radar and laser altimetry for the retrieval of sea ice thickness.

$$\rho_{ice} \cdot hi + \rho_{snow} \cdot hs = \rho_{water} \cdot (hi + hs - FB_s) \tag{1}$$

$$hi = \frac{\rho_{water}}{\rho_{water} - \rho_{ice}} \cdot FB_s - \frac{\rho_{water} - \rho_{snow}}{\rho_{water} - \rho_{ice}} \cdot hs \tag{2}$$

In this study, ρ_{water} and ρ_{ice} are taken to be 1024 kg/m^3 and $915 kg/m^3$ which are derived from field measurements discussed by Wadhams et al. (1992), and ρ_{snow} is 320 kg/m^3 derived from Warren et al. (1999).

3 Covariability between snow depth and snow freeboard and the effect on retrievability

We analyze the covariability between the snow depth (hs) and the snow freeboard (FB_s) on the scale of retrieval. Under the context of retrieval, we base the analysis with the freeboard measurements as a priori, and focus on how the snow depth changes with freeboard in a statistical sense. By using M available OIB samples that correspond to a single TB measurement, we show that there exists statistically significant correlation between the two data, and the relationship is better characterized by a nonlinear fitting. Furthermore, the effect of the covariability on retrievability is analyzed in Section 3.2.

3.1 Covariability analysis based on OIB data

For the covariability between FB_s and hs, we choose the native resolution of the OIB product (40 m) as the spatial scale for analysis. Each TB corresponds to multiple (M) OIB samples, with each sample containing the measurement for both FB_s and hs. We divide these samples into FB_s bins, with each bin covering 5 cm. In total there are 30 bins, covering the range of 0 to 1.5 m. For samples in each bin, we compute the percentiles and the mean value of hs. Figure 4.a shows the mean hs and the +/-1 standard deviation range and their relationship with FB_s, for 4 representative TB points. Furthermore, we carry out least squares fitting (weighted according to sample count in each bin) between mean hs and FB_s. Among all available TB and OIB data, there exist statistically significant positive correlation between hs and FB_s for over 90% of all points. The values of R^2 are in the range of 0.06 and 0.89 (95% percentile), with the mean value of R^2 as 0.53. This indicates that there exists consistent covariability between snow depth and snow freeboard across Arctic sea ice cover.

However, for both FYI and MYI ice, there is saturation of the mean snow depth with respect to the snow freeboard. Besides, in the Arctic inundation is generally uncommon (i.e., $hs < FB_s$). In order to accommodate these characteristics, we propose a nonlinear fitting as Equation 3. The parameters α and β are fitted according to observations which are both larger than 0. According to the equation, the value of hs saturates to $\alpha \cdot \pi/2$ with large values of FB_s, and the value of $\alpha \cdot \beta$ (denoted s) which is the slope of the function at $FB_s = 0$ should be lower than 1 in order to avoid inundation. Figure S4 and S5 (in part 2 of the supplementary material) show the statistics of α, β and s for FYI and MYI, respectively

$$hs(FB_s) = \alpha \cdot \arctan(\beta \cdot FB_s) \tag{3}$$

Using Equation 3, the overall quality of the fitting for all available local OIB segments is improved, with mean value of R^2 rising from 0.53 to 0.67, and the 95% percentile of R^2 rises to 0.23 and 0.92 respectively. Based on statistics of all the available OIB data, the value of s for the local OIB segment is in the range of 0.49 and 0.96 (95% percentile) with a single mode distribution for both MYI and FYI (Figure S4.c and S5.c). For FYI, the mean value of s is 0.71 and for MYI 0.95, which implies a generally thicker snow cover over MYI. Among all the local OIB segments, 80% of them witnessed a value of s lower than 1.

We consider the value of s to be stable across either FYI or MYI sea ice, and choose these values as universal parameters for the design of the retrieval algorithm. Figure 4.b shows fitting function of snow depth over snow freeboard based on these representative values of s under various values for α.

3.2 Effects on retrievability

We evaluate the covariability and its effect on retrieval from several aspects. We choose 5 realistic retrieval scenarios among all the OIB and SMOS data, with two of them representing FYI retrieval, and three of them for MYI. As shown in Table 1, they represent typical retrieval problems for Arctic sea ice. Besides, the simulated TB values by the radiation model is close to the corresponding SMOS TB values (within 1.5 K). Based on these scenarios, we examine whether it is possible to retrieve the actual sea ice thickness and snow depth, with or without the covariability. Firstly we ignore the covariability, and assume a flat snow cover. For all the M OIB samples, we assume that the snow depth is uniform. For the retrieval problem, since the directly observed values are freeboard samples ($FB_s|_m$, where m is the index of the samples, and $1 \leq m \leq M$), we carry out the scanning of the (uniform) snow depth hs from 0 m (snow free) to 1 m. Under a certain value of hs, we retrieve the sea ice thickness $hi|_m$ for each $FB_s|_m$ with Equation 2, based on the current value of hs. Then the TB value for this sample ($TB|_m$) can be calculated according to the L-band radiation model, with $hi|_m$, hs and surface temperature $T_{sfc}|_m$. The mean TB value is then computed as the arithmetic mean of all $TB|_m$'s, for the current value of hs. For any sample of FB_s, if the value of freeboard is smaller than the current value of hs, in order to avoid inundation, the snow depth for this sample is assumed to be the same as FB_s. If the number of samples that witness potential of inundation over 50 % of M, we stop the scanning even if hs has not reached 1 m.

In order to incorporate the effect of covariability, we adopt either the global value of s (0.71 for FYI and 0.95 for MYI) or the locally fitted value of s and carry out the retrieval. Figure 5.a shows 4 typical distribution of FB_s, and Figure 5.b shows a range of values for α (0 to 1) and the resulting mean value of hs for the 4 typical distributions. For the range of 0 to 1, the resulting mean hs covers a continuous range for each distribution. For each distribution, when α is very small, the corresponding hs is very small for whole range FB_s, resulting in a very small value of mean hs. Furthermore, the value of mean hs approaches 0 when α approaches 0, which in effect corresponds to the “bare-snow" case. With the grow of α, there exists monotonous increase in the mean hs, and when α is large enough, the mean hs saturates. For all of the 4 FB_s distributions, we consider that the resulting mean hs is reasonable for the range of α. Therefore, the retrieval of snow depth is attained by locating the proper value of α. Due to the potential of double solution in the retrieval, the solving of α is attained by a scanning process that cover the reasonable range for α. The scan starts from 0.001, steps by 0.01, and it is limited to a large value that yields saturation for mean hs. With each scanned value of α, a corresponding value for β can be computed as s/α, and the snow depth $hs|_m$ for each sample can be computed with Equation 3. Then the $hi|_m$, the TB values for each sample can be computed, as well as the mean snow depth and mean TB.

We record the (mean) snow depth, and the corresponding mean TB across the scanning process. Figure 6 shows the results of scanning for the five scenarios in Table 1. Note that for the lines that represent scanning of α (i.e., involving covariability), the x-axis is the resulting values of mean hs, not α. The observed TB and the simulated TB (with OIB data) are shown by solid

and dot-dashed horizontal lines, respectively. Besides, the observed mean snow depth and the 50 % inundation with flat snow cover are shown by solid and dashed vertical lines, respectively. The simulated TB with flat snow cover (black dashed curve in each subfigure) is always lower than that with covariability information (blue dashed curves for results with global s and red ones for those with local s). For all the scenarios, the TB values that are attained through scanning can reach the observed TB with the incorporation of covariability, while with the flat snow cover assumption, the values of TB in two scenarios (III and IV) fail to reach the observation. This implies that with the flat snow cover assumption, there is no solution to the retrieval problem. We further examine the other 3 scenarios, the solutions of the retrieval problem reside at the crosspoint of the scanned TB curves and the horizontal bars that represent observational TB values. The solutions of mean snow depth under the flat snow cover assumption are always larger than the observed mean snow depth by over 5 cm.

For the comparison between the covariability incorporated scanning with local s and global s, we show that for scenario I, II, III and IV, the solutions of the two scanning are close to each other (within 2 cm). For Scenario II, III and IV, the solutions as produced by the scanning is close to the observed snow depth. The differences between the solutions produced by scanning and the observed snow depth are 5 cm or larger for scenario I and V, with the scanning with local s produces smaller errors. It is worth noting that for the actual retrieval process, the local value of s is not available, and only the global value of s is usable. Lastly, for scenario III, two potential solutions exist (two crossing points between the TB scanning curve and the observational TB). Without extra observational data during retrieval, it is not possible to judge which solution is the true (or better) one. Therefore the retrieval algorithm should be able to locate both possible solutions.

The covariability as observed with OIB data plays an important role in the retrievability of the sea ice parameters. Also with OIB data, we extract the statistical relationship (Equation 3) that characterizes the covariability which can be incorporated in the retrieval. However, during retrieval, the parameter s is generally not available for the local sea ice cover, and the global values of s (for FYI and MYI) as computed from high-resolution OIB data can be adopted.

4 Retrieval algorithm and evaluation

In order to incorporate the covariability characteristics, we design the retrieval algorithm for sea ice thickness and snow depth that include two distinctive phases. The covariability feature is based on the nonlinear fitting in Equation 3 and the fixed value of s for both FYI and MYI sea ice as derived from OIB data. The first phase involves the scanning of possible snow depth configurations. This phase is in effect carried out by the scanning of the value of α from 0.001 to 3 (or sufficiently large). A possible solution is detected between two adjacent values of α, when the TB values as generated with these two values of α are on the different side of the observed TB. During the second phase, all the possible solutions are then computed with an iterative binary search of α. All possible solutions are reported by the retrieval algorithm. The outline of the algorithm is presented in Figure 7, with the two phases marked out by red and blue boxes, respectively. We also construct a reference retrieval algorithm based on the flat snow cover assumption, for which the scanning is over the snow depth instead of α. The details of this reference algorithm is omitted for brevity. We carry out the evaluation from two aspects, the retrieval with typical scenarios as presented in Section 3.2, as well as large-scale retrieval with available OIB data.

For the typical scenarios, we carry out the retrieval for the mean sea ice thickness ($\overline{Hi}$) and the mean snow depth ($\overline{Hs}$) using the standard algorithm with both global and local values of s, as well as the reference algorithm. Table 2 shows the comparison of the retrieval results and observations. The reference algorithm (with flat snow cover assumption) consistently performed worse than the standard algorithm. For scenario I and IV, it even failed to attain any solution. For the standard algorithm, the use of local value of s usually results in small errors in both $\overline{Hi}$ and $\overline{Hs}$. Also for scenario III for which two solutions are possible, the retrieval algorithm addresses both of them. The retrieval results are consistent with the retrievability analysis in Section 3.2.

In order to verify the algorithm, we carry out the retrieval with all the available OIB data (as mentioned in Section 2.3) which are from 35 OIB tracks and 412 SMOS TB measurements, and correspond to 412 retrieval cases. For each SMOS TB, the corresponding samples (snow freeboard, surface temperature and sea ice type) which are from OIB dataset are used for the retrieval. The retrieval with the flat snow cover assumption (the reference algorithm) is only successful for 50 cases, which accounts for about 12 % of available cases. For comparison, the (standard) algorithm achieves retrieval for 391 cases (95%) with the global s values, and for all the TB values with the locally fit s values. Figure 8 shows the comparison of retrieved mean sea ice thickness and snow depth with observations. Figure 8.a and b shows the results for sea ice thickness and snow depth, based on: (1) simulated TB (as computed from the radiation model), and (2) the local value of s. This represent the most "ideal" retrieval case in which there exists no extra uncertainty. As shown in Figure 8.a, the LSQ fit for $\overline{Hi}$ (dash line) features a R^2 value of 0.966, while the LSQ fit under the extra constraint on slope (dotted dash line) features a R^2 value of 0.964. Also for snow depth (Figure 8.b), the R^2 values for the two fittings are both 0.844. This indicates that the retrieval is in good agreement with the observations.

For the actual retrieval problem for which the local value of s is unknown and the observational TB values from SMOS, Figure 8.c and d shows the evaluation for sea ice thickness and snow depth respectively. The fitting quality (in terms of R^2) for sea ice thickness is as high as 0.89 and that for snow depth is 0.637. It is worth noting that these results are achieved with only statistical data derived from large-scale OIB surveys. Furthermore, if the retrieval is based on: (1) observed TB from SMOS, and (2) the locally fitted value of s, the R^2 values for the fitting are 0.91 and 0.65 for sea ice thickness and snow depth respectively, with virtually no change in the fitting lines (not shown). There is minor increase in quality (0.91 versus 0.89 and 0.65 versus 0.637) and a relatively large gap to the "ideal" case. As a comparison, we also carry out retrieval with the TB with forward model and the local values of s, and the R^2 for fittings between the retrieved and the observed parameters for sea ice thickness and snow depth are 0.96 and 0.84, respectively. This indicates that the difference (or error) of the modeled and the observed TB plays an important role in affecting the quality of the retrieval. The uncertainty of TB may arise from that of the radiation model, as well as the mismatch between the altimetry and passive microwave remote sensing, as introduced in Section 2.2.

For comparison, we carry out comparison with the idealized scenario of retrieval which only involves TB and the mean value of FB_s. This idealized scenario in Xu et al. (2017) ignores the resolution difference between altimetry scans and L-band radiometry, and it represents a theoretical study of the retrieval problem. Specifically, for the use of OIB data, the mean value of M samples of FB_s is computed, and further combined with TB for the retrieval of a single value of sea ice thickness and

snow depth. Since only the mean FB_s is involved in the retrieval, covariability does not play a role in the retrieval. By using the same SMOS and OIB data as the evaluation in Figure 8, the retrieval yields R^2 of 0.78 and 0.50 for hi and hs (fitting between the retrieved and the observed parameter). For a comparison, under the realistic scenario which involves multiple altimetry scans for a single TB (Figure 8.c and d), the quality of retrieval is much improved for both hi (R^2 from 0.78 to 0.89) and hs (R^2 from 0.50 to 0.64). This demonstrates that the high-resolution altimetry samples and the accompanying covariability information play an important role in improving the retrieval, as compared with the idealized retrieval scenario in Xu et al. (2017).

Based on the retrieval with large-scale observational data, the proposed algorithm achieves effective retrieval of both sea ice thickness and snow depth, by using simultaneous remote sensing of the sea ice cover, i.e., laser altimetry and L-band passive microwave sensing. The statistics of snow depth and its covariability with snow freeboard on the spatial scale of retrieval play an important role in improving the well-posedness of the retrieval problem, as well as the quality of the retrieved parameters.

5 Summary and discussion

In this study, we introduce a novel algorithm for retrieving multiple Arctic sea ice parameters based on combination of L-band passive microwave remote sensing and active laser altimetry. Two physical models, the L-band radiation model and the buoyancy relationship, are adopted to constrain the sea ice thickness and snow depth. They are used as forward models during an iterative retrieval process that solves the sea ice parameters that satisfy the observed L-band TB and snow freeboard values. Specifically, according to observations, there exists covariability between the snow depth and the snow freeboard which are the objective and the input for the retrieval, respectively. The covariability plays a key role in the retrievability, and therefore should be incorporated in the retrieval algorithm. A nonlinear fitting that characterizes the covariability is derived from OIB data, and a parameter (initial slope of the fitting function) is considered to be stable among large-scale observations. This set of parameters (for FYI and MYI respectively) is adopted in the retrieval algorithm. Verification with available OIB data shows that the retrieval is attained for both sea ice thickness and snow depth, with the uncertainty mainly arising from the mismatch between modeled and observed TB values. This algorithm can be applied to the large-scale retrieval of sea ice thickness and snow depth using concurrent L-band satellite remote sensing and satellite altimetry of the sea ice cover such as Abdalati et al. (2010).

There are key differences between the proposed algorithm with existing retrieval methods. In traditional (laser) satellite altimetry, the retrieval of sea ice thickness mainly relies on (adapted) climatological snow depth or data as derived from reanalyses, which may contain unconstrained uncertainty due to model biases as well as missing physical processes. Besides, these snow depth data usually lack fine-scale details that match the resolution of satellite altimetry, such as the covariability characteristics. On the other hand, the retrieval of snow depth using L-band SMOS data as in Maaß et al. (2013b) relies on the a priori knowledge of the thickness of the (thick) sea ice. Contrary to these existing retrieval algorithms, the proposed algorithm carries out retrieval of both sea ice thickness and snow depth, with the concurrent active and passive remote sensing of the sea

ice cover. Since no climatological snow depth or any other derived snow data is used in the algorithm, the retrieved sea ice thickness do not suffer from the potential lack of efficacy of these data.

In Kwok et al. (2011), statistical analyses are carried out between snow depth and snow freeboard, which also show covariability between the two. However, it is worth noting that the scale and the resolution as adopted in Kwok et al. (2011) are about 400 km and 4 km, respectively. They are both much larger than the those as used in this study (about 40 km and 40 m). While the analyses in Kwok et al. (2011) is on coarser spatial scales, our work focuses on the spatial scale that is relevant to the retrieval of sea ice parameters. We demonstrate that on this relatively small spatial scale, there still exists covariability between snow depth and snow freeboard.

The proposed retrieval method is the basis for the retrieval of sea ice parameters with data from concurrent satellite campaigns. Although there was no concurrent L-band satellite observation with the ICESat campaign, there are candidate satellite campaigns such as WCOM (Shi et al., 2016) that provides concurrent L-band observation with the planned ICESat-2 campaign. For the study with satellite data, there exist several practical issues. First, the snow surface temperature is provided by airborne sensors in OIB, but not generally available with laser altimetry. Several data sources serve as candidate data for the concurrent surface temperature field, such as reanalysis data (Dee et al., 2011), MODIS based product (Hall et al., 2004). Second, there exists small-scale variability of the sea ice cover such as leads, which were not considered for the analysis and verification in this study. As shown in Zhou et al. (2017), the presence of sea ice leads has profound effect in lowering the overall TB on the scale of SMOS observations. Leads can be treated as small-scale heterogeneity of the sea ice cover, and the incorporation of lead maps such as Willmes and Heinemann (2015b) effectively reduces the overestimation of TB, as studied in Zhou et al. (2017). Specifically, the lead map can be adopted by the retrieval through the integration with the forward radiation model. Other types of small scale variability such as mixture of FYI and MYI, should be also accounted for using sea ice type maps. Third, the covariability explored in this study is on the spatial scale of the original OIB data (i.e., 40 m). For each specific satellite altimetry, we consider the freeboard measurement the mean freeboard value within a certain spatial range. For ICESat-2, each laser scan dot covers a circular region of about 70 m in diameter (Abdalati et al., 2010). The scaling of the covariability should be studied for the specific resolution of the satellite altimetry. By using 70 m as the typical resolution of ICESat-2, we deduce the value of s at this resolution by manual coarsening OIB's data by averaging adjacent points. In effect, the value of s at 80 m is computed, which shows a slight decrease of s for both FYI and MYI. Figure S6 (in part 2 of the supplementary material) shows the general scaling of s for the resolution range from 40 m to 240 m. Fourth, in order to estimate the uncertainty of the retrieved parameters, the effects of surface temperature, as well as other data sources (including TB, freeboard measurements, and the value of s), should be evaluated in a systematic way. Due to the nonlinear relationship between TB and the sea ice parameters, Monte-Carlo simulations can be carried out for the quantification of the uncertainty. Besides, for the historical data from from ICESat (Kwok and Cunningham, 2008) during the first decade of the 21st century, due to the lack of basin-scale L-band observation for the Arctic, other passive remote sensing data such as C-band data from AMSR-2 can be exploited in a similar manner for the retrieval of these historical data.

Acknowledgements. This work is partially supported by National Key R & D Program of China under the grant number of 2017YFA0603902 and the General Program of National Science Foundation of China under the grant number of 41575076. The authors would like to thank the editors and referees for their invaluable efforts in improving the manuscript. SMOS data is provided from Integrated Climate Data Center (ICDC), icdc.cen.uni-hamburg.de, University of Hamburg, Germany, Digital media. http://icdc.cen.uni-hamburg.de/1/daten/cryosphere/l3b-smos-tb.html. [Data Accessed: 2017/10/25]. OIB and SSM/I sea ice concentration data are provided by NASA National Snow and Ice Data Center Distributed Active Archive Center, Boulder, Colorado USA. doi: http://dx.doi.org/10.5067/7XJ9HRV50O57. [Data Accessed: 2017/10/25]. Besides, the authors are grateful to Willmes, S. and Heinemann, G. for the provision of Arctic sea ice lead map.

References

Aaboe, S., Breivik, L.-A., Eastwood, S., and Sorensen, A.: Sea Ice Edge and Type Products, http://osisaf.met.no/p/ice/edge_type_long_description.html, accessed: 2016-12-30, 2016.

Abdalati, B., Zwally, H., Bindschadler, R., Csatho, B., Farrell, S., Fricker, H., Harding, D., Kwok, R., Lefsky, M., Markus, T., Marshak, A., Neumann, T., Palm, S., Schutz, B., Smith, B., Spinhirne, J., and Webb, C.: The ICESat-2 laser altimetry mission, in: Proc. IEEE, vol. 98, pp. 735–751, doi:10.1109/JPROC.2009.2034765, 2010.

Brucker, L. and Markus, T.: Arctic-scale assessment of satellite passive microwave-derived snow depth on sea ice using Operation IceBridge airborne data, Journal of Geophysical Research: Oceans, 118, 2892–2905, 2013.

Burke, W., Schmugge, T., and Paris, J.: Comparison of 2.8-and 21-cm microwave radiometer observations over soils with emission model calculations, Journal of Geophysical Research: Oceans, 84, 287–294, 1979.

Cavalieri, D., Parkinson, C., Gloersen, P., and Zwally, H.: Sea Ice Concentrations from Nimbus-7 SMMR and DMSP SSM/I-SSMIS Passive Microwave Data, Boulder, Colorado USA. NASA National Snow and Ice Data Center Distributed Active Archive Center. doi: http://dx.doi.org/10.5067/8GQ8LZQVL0VL., 1996.

Cavalieri, D. J., Parkinson, C. L., Gloersen, P., Comiso, J. C., and Zwally, H. J.: Deriving long-term time series of sea ice cover from satellite passive-microwave multisensor data sets, Journal of Geophysical Research: Oceans, 104, 15 803–15 814, 1999.

Comiso, J., Cavalieri, D., and Markus, T.: Sea ice concentration, ice temperature, and snow depth using AMSR-E data, IEEE Trans. Geosci. Remote Sens., 41, 243–252, 2003.

Comiso, J. C., Parkinson, C. L., Gersten, R., and Stock, L.: Accelerated decline in the Arctic sea ice cover, Geophysical research letters, 35, 2008.

Dee, D., Uppalaa, S., Simmonsa, A., Berrisforda, P., Polia, P., Kobayashib, S., Andraec, U., Balmasedaa, M., Balsamoa, G., Bauera, P., Bechtolda, P., Beljaarsa, A., van de Berg, L., Bidlota, J., Bormanna, N., Delsola, C., Dragania, R., Fuentesa, M., Geera, A., Haimbergere, L., Healya, S., Hersbacha, H., Holma, E., Isaksena, L., Kallbergc, P., Kohlera, M., Matricardia, M., McNallya, A., Monge-Sanzf, B., Morcrettea, J.-J., Parkg, B.-K., Peubeya, C., de Rosnaya, P., Tavolatoe, C., Thepauta, J.-N., and Vitart, F.: The ERA-Interim reanalysis: configuration and performance of the data assimilation system, Quarterly Journal of the Royal Meteorological Society, 137, 553–597, 2011.

Hall, D., Key, J., Casey, K., Riggs, G., and Cavalieri, D.: Sea ice surface temperature product from MODIS, IEEE T. Geosci. Remote, 42, 1076–1087, 2004.

Kaleschke, L., Maaß, N., Haas, C., Hendricks, S., Heygster, G., and Tonboe, R.: A sea-ice thickness retrieval model for 1.4 ghz radiometry and application to airborne measurements over low salinity sea-ice, The Cryosphere, 4, 583–592, 2010.

Krabill and B., W.: IceBridge ATM L1B Qfit Elevation and Return Strength, [indicate subset used], Boulder, Colorado USA: NASA DAAC at the National Snow and Ice Data Center. http://dx.doi.org/10.5067/DZYN0SKIG6FB, updated 2013, 2009.

Kurtz, N., Markus, T., Farrell, S., Worthen, D., and Boisvert, L.: Observations of recent Arctic sea ice volume loss and its impact on ocean-atmosphere energy exchange and ice production, Journal of Geophysical Research: Oceans, 116, 2011.

Kurtz, N. T. and Farrell, S. L.: Large-scale surveys of snow depth on Arctic sea ice from Operation IceBridge, Geophysical Research Letters, 38, doi:10.1029/2011GL049216, http://dx.doi.org/10.1029/2011GL049216, l20505, 2011.

Kurtz, N. T., Farrell, S. L., Studinger, M., Galin, N., Harbeck, J. P., Lindsay, R., Onana, V. D., Panzer, B., and Sonntag, J. G.: Sea ice thickness, freeboard, and snow depth products from Operation IceBridge airborne data, The Cryosphere, 7, 1035–1056, doi:10.5194/tc-7-1035-2013, www.the-cryosphere.net/7/1035/2013/, 2013.

Kwok, R. and Cunningham, G. F.: ICESat over Arctic sea ice: Estimation of snow depth and ice thickness, Journal of Geophysical Research: Oceans, 113, doi:10.1029/2008JC004753, http://dx.doi.org/10.1029/2008JC004753, c08010, 2008.

Kwok, R., Cunningham, G. F., Wensnahan, M., Rigor, I., Zwally, H. J., and Yi, D.: Thinning and volume loss of the Arctic Ocean sea ice cover: 2003-2008, Journal of Geophysical Research: Oceans, 114, doi:10.1029/2009JC005312, http://dx.doi.org/10.1029/2009JC005312, c07005, 2009.

Kwok, R., Panzer, B., Leuschen, C., Pang, S., Markus, T., Holt, B., and Gogineni, S.: Airborne surveys of snow depth over Arctic sea ice, Journal of Geophysical Research: Oceans, 116, 2011.

Laxon, S., Peacock, N., and Smith, D.: High interannual variability of sea ice thickness in the Arctic region, Nature, 425, 947, 2003.

Laxon, S. W., Giles, K. A., Ridout, A. L., Wingham, D. J., Willatt, R., Cullen, R., Kwok, R., Schweiger, A., Zhang, J., Haas, C., Hendricks, S., Krishfield, R., Kurtz, N., Farrell, S., and Davidson, M.: CryoSat-2 estimates of Arctic sea ice thickness and volume, Geophysical Research Letters, 40, 732–737, doi:10.1002/grl.50193, 2013.

Leuschen, C.: IceBridge Snow Radar L1B Geolocated Radar Echo Strength Profiles, Version 2. [Indicate subset used], Boulder, Colorado USA. NASA National Snow and Ice Data Center Distributed Active Archive Center. doi: http://dx.doi.org/10.5067/FAZTWP500V70, updated 2017, 2014.

Maaß, N., Kaleschke, L., and Stammer, D.: Remote sensing of sea ice thickness using SMOS data, Ph.D. thesis, University of Hamburg Hamburg, 2013a.

Maaß, N., Kaleschke, L., Tian-Kunze, X., and Drusch, M.: Snow thickness retrieval over thick Arctic sea ice using SMOS satellite data, The Cryosphere, 7, 1971–1989, doi:10.5194/tc-7-1971-2013, www.the-cryosphere.net/7/1971/2013/, 2013b.

McPhee, M., Proshutinsky, A., Morison, J. H., Steele, M., and Alkire, M.: Rapid change in freshwater content of the Arctic Ocean, Geophysical Research Letters, 36, 2009.

Perovich, D., Jones, K., Light, B., Eicken, H., Markus, T., Stroeve, J., and Lindsay, R.: Solar partitioning in a changing Arctic sea-ice cover, Annals of Glaciology, 52, 192–196, 2011.

Rothrock, D. A., Yu, Y., and Maykut, G. A.: Thinning of the Arctic sea-ice cover, Geophysical Research Letters, 26, 3469–3472, 1999.

Screen, J. A. and Simmonds, I.: The central role of diminishing sea ice in recent Arctic temperature amplification, Nature, 464, 1334, 2010.

Shetter, R., Buzay, E., and Gilst., D. V.: IceBridge NSERC L1B Geolocated Meteorologic and Surface Temperature Data, Version 1. [Indicate subset used]., Boulder, Colorado USA. NASA National Snow and Ice Data Center Distributed Active Archive Center. doi: http://dx.doi.org/10.5067/Y6SQDAAAOEQU., updated 2013, 2010.

Shi, J., Dong, X., Zhao, T., Du, Y., Liu, H., Wang, Z., Zhu, D., Ji, D., Xiong, C., and Jiang, L.: The water cycle observation mission (WCOM): Overview, in: 2016 IEEE International Geoscience and Remote Sensing Symposium (IGARSS), pp. 3430–3433, doi:10.1109/IGARSS.2016.7729886, 2016.

Stocker, T. F., Qin, D., Plattner, G.-K., Tignor, M., Allen, S. K., Boschung, J., Nauels, A., Xia, Y., Bex, V., Midgley, P. M., et al.: Climate change 2013: The physical science basis, Intergovernmental Panel on Climate Change, Working Group I Contribution to the IPCC Fifth Assessment Report (AR5)(Cambridge Univ Press, New York), 2013.

Stroeve, J., Barrett, A., Serreze, M., and Schweiger, A.: Using records from submarine, aircraft and satellites to evaluate climate model simulations of Arctic sea ice thickness, The Cryosphere, 8, 1–16, doi:10.5194/tc-8-1-2014, 2014.

Stroeve, J. C., Serreze, M. C., Holland, M. M., Kay, J. E., Malanik, J., and Barrett, A. P.: The Arctic's rapidly shrinking sea ice cover: a research synthesis, Climatic Change, 110, 1005–1027, 2012.

Tian-Kunze, X., Kaleschke, L., Maaß, N., Serra, M. M. N., Drusch, M., and Krumpen, T.: SMOS-derived thin sea ice thickness: algorithm baseline, product specifications and initial verification, The Cryosphere, 8, 997–1018, doi:10.5194/tc-8-997-2014, www.the-cryosphere.net/8/997/2014/, 2014.

Tilling, R. L., Ridout, A., Shepherd, A., and Wingham, D. J.: Increased Arctic sea ice volume after anomalously low melting in 2013, Nature Geoscience, 8, 643–646, 2015.

Toudal Pedersen, L., Dybkjær, G., Eastwood, S., Heygster, G., Ivanova, N., Kern, S., Lavergne, T., Saldo, R., Sandven, S., Sørensen, A., and Tonboe, R.: ESA Sea Ice Climate Change Initiative(Sea_Ice_cci): Sea Ice Concentration Climate Data Record from the AMSR-E and AMSR-2 instruments at 25km grid spacing, version 2.0., Centre for Environmental Data Analysis, 28 February 2017, doi:10.5285/c61bfe88-873b-44d8-9b0e-6a0ee884ad95, accessed: 2017-5-30, 2017.

Wadhams, P., III, W. T., Krabill, W., Swift, R., Comiso, J., and Davis, N.: Relationship between sea ice freeboard and draft in the Arctic basin, and implications for ice thickness monitoring, J. Geophys. Res, 97, 1992.

Warren, S. G., Rigor, I. G., Untersteiner, N., Radionov, V. F., Bryazgin, N. N., Aleksandrov, Y. I., and Colony, R.: Snow Depth on Arctic Sea Ice, Journal of Climate, 12, 1814 – 1829, doi:10.1175/1520-0442(1999)012<1814:SDOASI>2.0.CO;2, http://dx.doi.org/10.1175/1520-0442(1999)012<1814:SDOASI>2.0.CO;2, 1999.

Webster, M. A., Rigor, I. G., Nghiem, S. V., Kurtz, N. T., Farrell, S. L., Perovich, D. K., and Sturm, M.: Interdecadal changes in snow depth on Arctic sea ice, Journal of Geophysical Research: Oceans, 119, 5395–5406, doi:10.1002/2014JC009985, http://dx.doi.org/10.1002/2014JC009985, 2014.

Willmes, S. and Heinemann, G.: Pan-Arctic lead detection from MODIS thermal infrared imagery, Annals of Glaciology, 56, 29–37, 2015a.

Willmes, S. and Heinemann, G.: Sea-ice wintertime lead frequencies and regional characteristics in the Arctic, 2003-2015, Remote Sensing, 8, 2015b.

Xu, S., Zhou, L., Liu, J., Lu, H., and Wang, B.: Data Synergy between Altimetry and L-Band Passive Microwave Remote Sensing for the Retrieval of Sea Ice Parameters - A Theoretical Study of Methodology, Remote Sensing, 9, doi:10.3390/rs9101079, 2017.

Zhou, L., Xu, S., Liu, J., Lu, H., and Wang, B.: Improving L-band radiation model and representation of small-scale variability to simulate brightness temperature of sea ice, International Journal of Remote Sensing, 38, 7070–7084, doi:10.1080/01431161.2017.1371862, http://dx.doi.org/10.1080/01431161.2017.1371862, 2017.

Zygmuntowska, M., Rampal, P., Ivanova, N., and Smedsrud, L. H.: Uncertainties in Arctic sea ice thickness and volume: new estimates and implications for trends, The Cryosphere, 8, 705 – 720, doi:10.5194/tc-8-705-2014, www.the-cryosphere.net/8/705/2014/, 2014.

Competing interests. The authors declare no conflict of interest

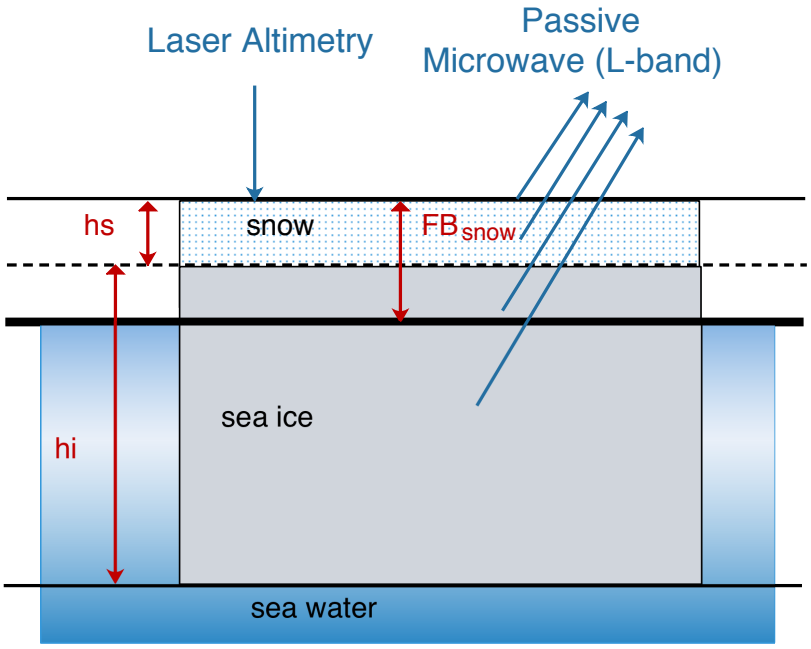

Figure 1. Sea ice parameters in the active and passive remote sensing of the sea ice cover, including sea ice thickness (hi), snow depth (hs) and snow freeboard (FB_s).

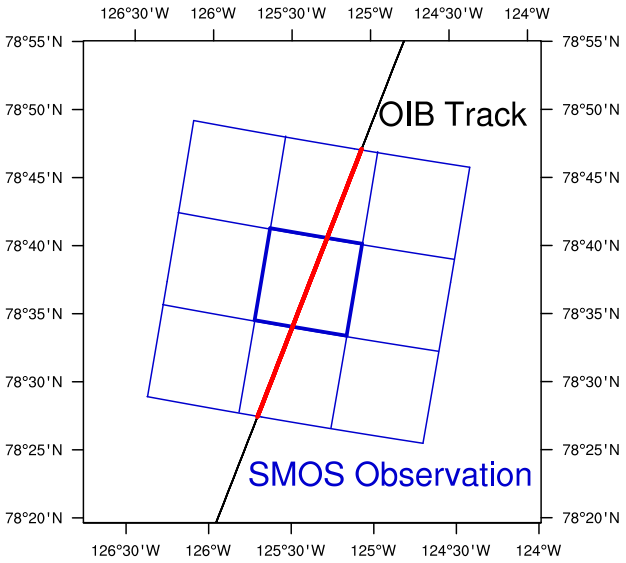

Figure 2. Data match between OIB and SMOS data. SMOS TB product is provided on the 12.5 km EASE grid (shown by blue rectangular cells). However, the inherent resolution of SMOS TB is of about 40 km. The red/black line represents the OIB track. Therefore, in order to accommodate the resolution differences, OIB samples that reside within the 9 cells (red) are considered to be of equal contribution to the TB value at the central EASE grid cell (outline by the thick blue line).

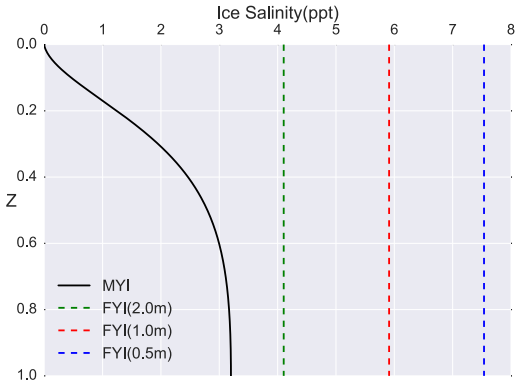

(a) Vertical salinity profile

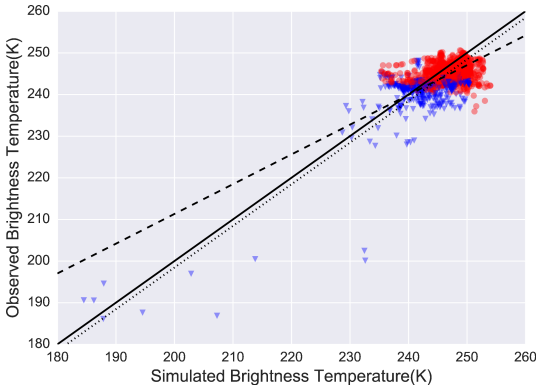

(b) Verification of sea ice radiation model

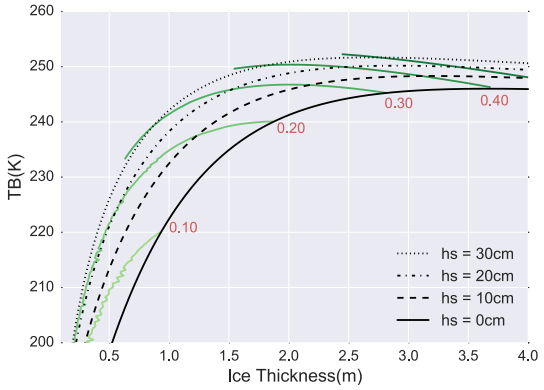

(c) Relationship between TB and sea ice thickness and corresponding FB_s

Figure 3. L-band radiation model. Subfigure a shows sea ice salinity profile for FYI (dotted lines) and MYI (solid line). The vertical axis (Z) is normalized with respect to the sea ice thickness. The comparison of the simulated TB based on OIB data and the observed SMOS TB is presented in subfigure b. Blue triangles represent FYI, while red circles MYI. The dashed (dotted) line is the least squares fit (least squares fit under the constraint that slope be 1). The Root Mean Square Error of TB is 3 K. Subfigure 3 shows the modeled TB under typical parameters (sea ice thickness and snow depth) and sea ice thermal conditions (surface temperature of -30 $^{\circ}C$). The green lines represent constant snow freeboard lines.

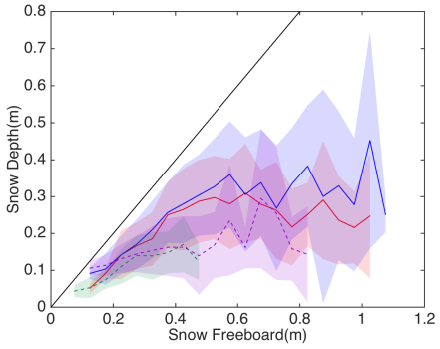

(a) Total freeboard and snow depth

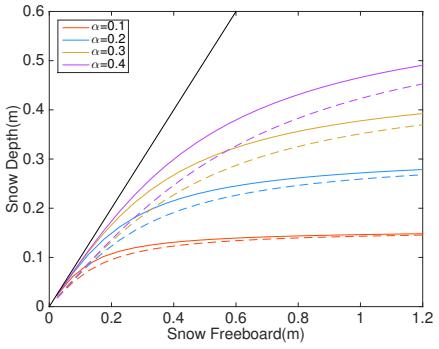

(b) Functional fitting for snow depth

Figure 4. Statistics of snow depth from OIB at the local scale of retrieval. Subfigure a shows the mean and the $+/-1$ standard deviation of the snow depth within each snow freeboard bin (from 0 m to 1.5 m by the interval of 5 cm), shown by lines and shaded areas for 4 realistic cases of OIB. Subfigure b shows the the nonlinear fitting of snow depth over snow freeboard (Equation 3) under representative s values (0.71 for FYI and 0.95 for MYI) and various values of α. Solid color lines are for MYI and dashed ones for FYI. The solid black line is $y = x$.

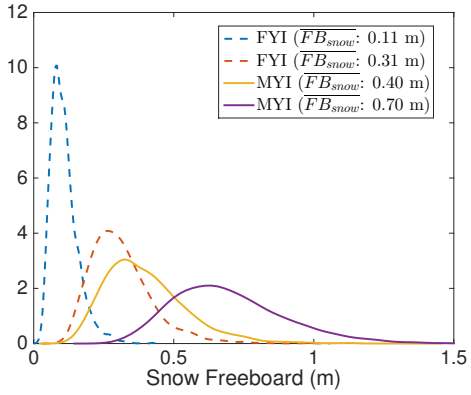

(a) 4 typical distributions of FB_s

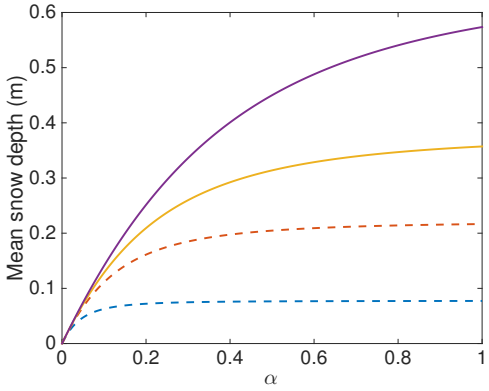

(b) Derived mean hs with respect to the values for α

Figure 5. Typical distributions of FB_s and the range of mean hs for $0 < \alpha < 1$. Subfigure a shows the 4 distributions (2 for FYI and 2 for MYI) and the corresponding mean value of FB_s. Global values of s for FYI and MYI are adopted. For these 4 distributions, subfigure b shows the mean hs for the range of α between 0 and 1. Mean hs increases monotonically with α, and saturates when α is large

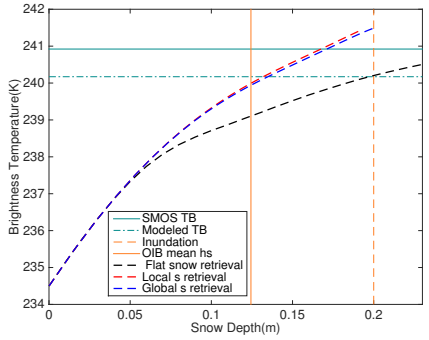

(a) Scenario I

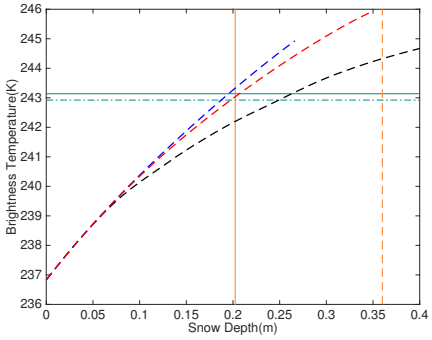

(b) Scenario II

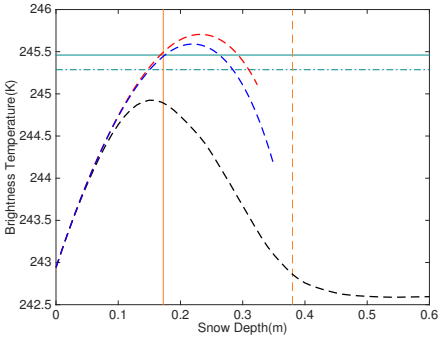

(c) Scenario III

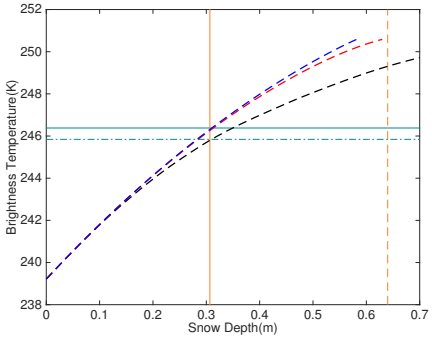

(d) Scenario IV

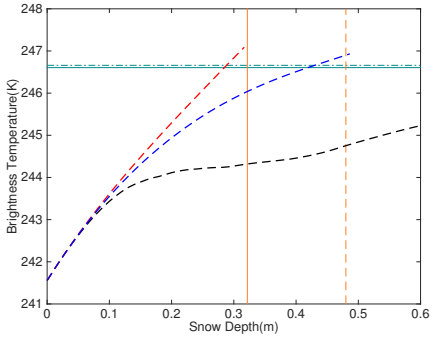

(e) Scenario V

Figure 6. Retrievability study with different retrieval scenarios. The horizontal solid (dotted-dashed) lines are the SMOS (modeled) TB. The vertical solid lines represent the values of the mean snow depth from OIB observation. The black dashed curves denote the values of TB generated by scanning of hs under the flat snow cover assumption, and the vertical dashed lines denote the values of hs that result in 50% OIB samples to be inundated. The red (blue) dashed curves (with the corresponding mean snow depth) are the values of TB generated by scanning of α with the local (global) values of s as in Equation 3.

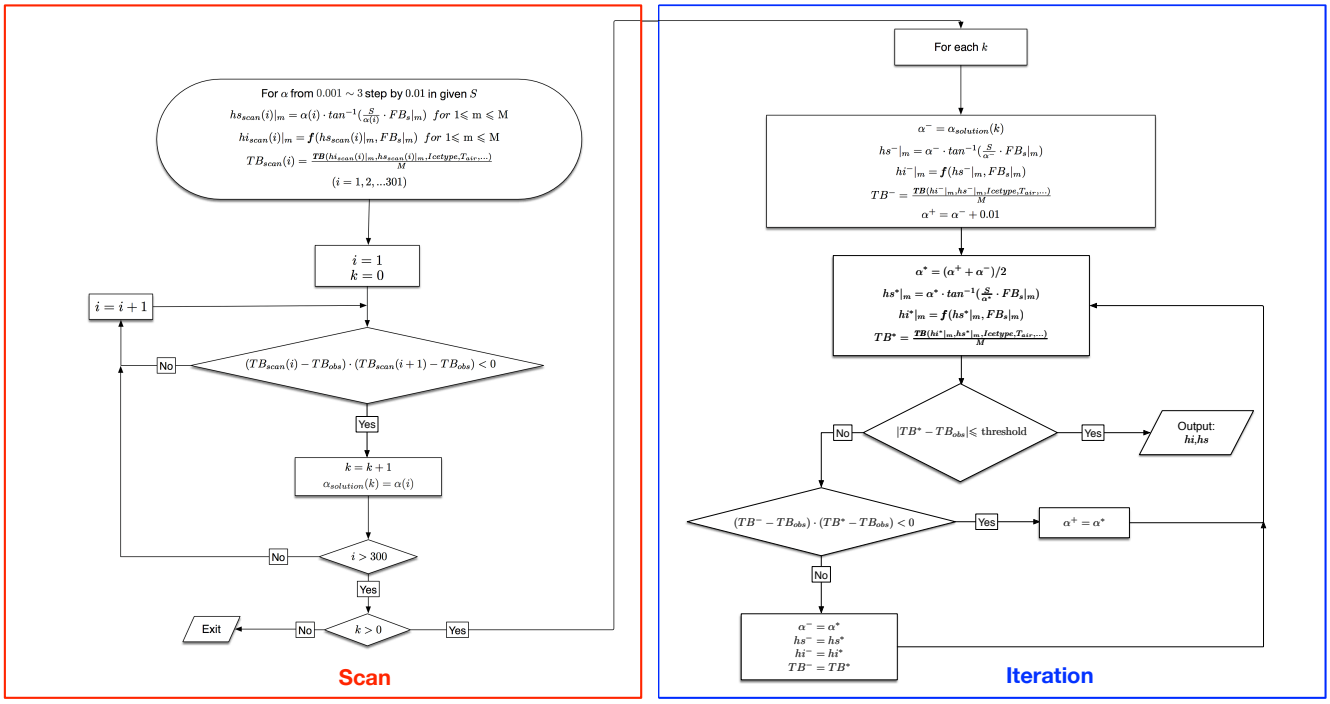

Figure 7. Flow chart for retrieval algorithm. Two phases are marked out. The red box includes the scanning process for the potential solutions to the retrieval problem, and the blue box the iterative binary search for the solving process.

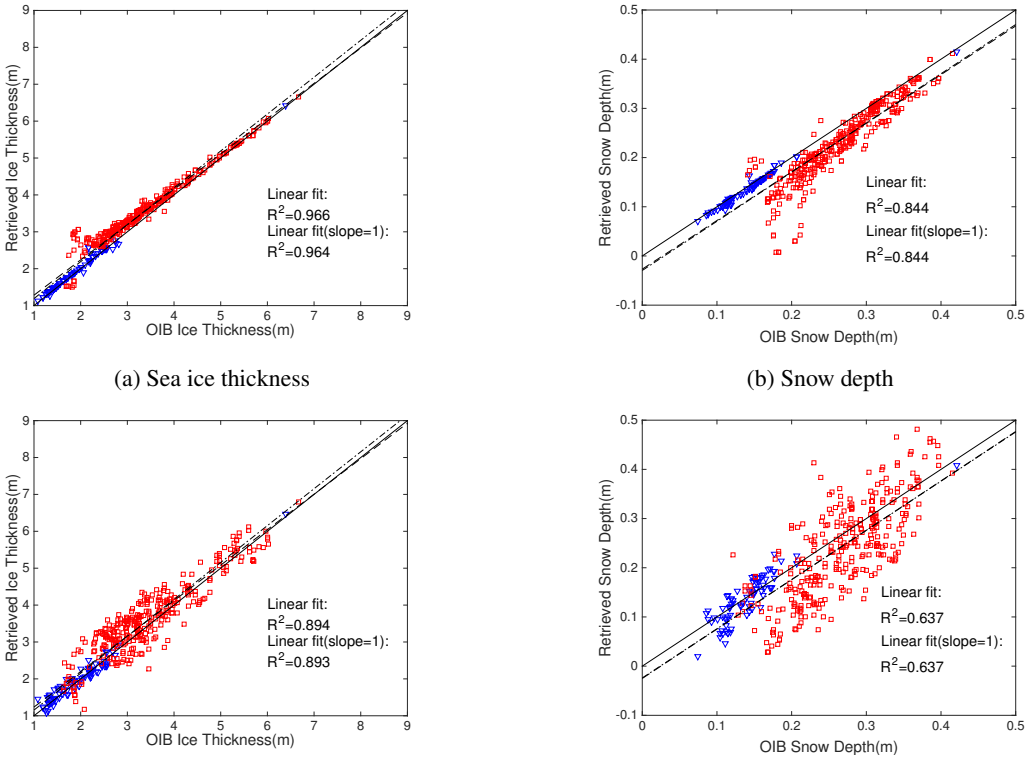

(a) Sea ice thickness

(b) Snow depth

(c) Sea ice thickness

(d) Snow depth

Figure 8. Large-scale retrieval of mean sea ice thickness (subfigure a and c) and mean snow depth (subfigure b and d) and verification with OIB observations. In each subfigure: blue triangles (red rectangles) denote FYI (MYI); the solid line is the 1:1 line; the dashed (dashed dotted) line represents the linear fitting (linear fitting line with the constraint that the slope be 1). The quality of fittings in terms of R^2 are also shown. Subfigure a and b represent the comparison results for the retrieval with modeled TB and the local values of s. Subfigure c and d represent the results with SMOS TB and the global values of s as derived from OIB data.

Table 1. Typical retrieval scenarios. The mean sea ice thickness ($\overline{Hi}$), mean snow depth ($\overline{Hs}$), mean snow freeboard ($\overline{FBs}$), observed TB from SMOS and the simulated TB from forward radiation model are shown. Scenario I and II are FYI, and scenario III, IV and V are MYI.

Ice type	Scenario	$\overline{Hi}\,(m)$	$\overline{Hs}\,(m)$	$\overline{FB_s}\,(m)$	$TB\,(K)$	
					Simulated	Observed
FYI	I	1.28	0.12	0.2212	245.84	246.38
	II	2.25	0.20	0.3790	242.92	243.14
MYI	III	2.46	0.17	0.3807	245.29	245.46
	IV	3.01	0.32	0.5419	246.66	246.61
	V	4.13	0.31	0.6509	245.84	246.38

Table 2. Retrieved results ($\overline{Hs}$ and $\overline{Hs}$, in units of meters) for five scenarios under different retrieval algorithms. In scenario II, IV and V, the retrieval with flat snow cover assumption is unsuccessful. The values in the brackets for scenario V denote the other (possible) solution for sea ice parameters.

Scenario	$\overline{Hi}\ (m)$				$\overline{Hs}\ (m)$			
	Observed	Retrieval w/ flat snow cover	Retrieval w/ local s	Retrieval w/ global s	Observed	Retrieval w/ flat snow cover	Retrieval w/ local s	Retrieval w/ global s
I	1.28	–	0.95	0.93	0.124	–	0.167	0.171
II	2.25	2.00	2.23	2.30	0.202	0.263	0.207	0.195
III	2.46	–	2.50 (1.69)	2.45 (1.88)	0.172	–	0.168 (0.293)	0.175 (0.263)
IV	3.01	–	3.25	2.38	0.321	–	0.285	0.419
V	4.13	3.88	4.09	4.11	0.308	0.350	0.313	0.310

Content of the supplementary material

Part 1: Introduction of the L-band radiation model

Part 2: Statistics for the covariability between FB_s and *hs*

Part 1: Introduction of the L-Band Radiation Model for Sea Ice

The L-band (1.4 GHz) radiation model as used for retrieval describes the radiation emitted from snow covered sea ice that floats over sea water. The model was originally developed for soil moisture applications in Burke et al. (1979), and further adopted for sea ice in Maaß et al. (2013a). As introduced in Zhou et al., (2017), improvements to the model are made to better characterize the vertical structure of the sea ice that is specific to each sea ice type. Details are provided below.

1. General information

The modeling of the radiative properties of the sea ice cover include 4 types of media in the vertical direction: the sea water beneath the sea ice, the sea ice, the snow cover over the sea ice, and the air. The sea water (air) are considered to be semi-infinite beneath (above) the sea ice cover. The sea ice is further divided into *N* layers in the vertical direction, with each layer of the same height. For the snow cover, a homogeneous structure is assumed, with prescribed thermal conductivity, etc. Besides, dry snow is assumed, and snow morphology features (such as differentiation between wind slab and depth hoar) and similar inhomogeneous vertical structure are not considered. The (SMOS) observed brightness temperature (TB) is assumed to be the multi-angle mean (0-40 degrees) TB as radiated from the aforementioned multi-layer media.

2. Temperature and salinity structure

The radiation model characterizes the vertical structure of the sea ice cover, by specifying the temperature and salinity of each layer, according to other supportive data such as sea ice type, snow surface temperature, etc.

The vertical temperature profile is determined by the overall thermal condition (in terms of the snow surface temperature, T_{surf}), and the thermal conductivity for sea ice (k_{ice}) and that of snow (k_{snow}). The bottom of the sea ice is assumed to be at freezing temperature of -1.8 ℃ (denoted T_{water}). Based on fittings with observations in Untersteiner (1964) and Yu and Rothrock (1996), the thermal conductivity is defined as:

$$k_{ice} = 2.034\, Wm^{-1}K^{-1} + 0.13\, Wkg^{-1}m^{-2}\frac{S_{ice}}{T_{ice} - 273.15}$$

$$k_{snow} = 0.31 Wm^{-1}K^{-1}$$

In this study, we consider the change of k_{ice} within the sea ice of minor effects, and use a bulk value for k_{ice}, resulting in a linear temperature profile within the sea ice. This bulk value is determined by the bulk value of S_{ice}. The temperature profile is assumed to be continuous through the media interfaces, and ice temperature is assumed to equal the snow temperature at the snow–ice interface. Given T_{surf} which may be derived from other observations (such as MODIS), the bulk ice and snow temperatures T_{ice} and T_{snow} can be written as:

$$T_{ice} = T_{water} + \frac{1}{2}K(T_{surf} - T_{water})k_{snow}h_{ice}$$

$$T_{snow} = \frac{1}{2}(T_{water} + T_{surf} + K(T_{surf} - T_{water})k_{ice}h_{snow})$$

where h_{ice} is the sea ice thickness and h_{snow} is the snow depth and $K = (k_{snow}h_{ice} + k_{ice}h_{snow})^{-1}$. Since a bulk value is adopted for both k_{ice} and k_{snow}, given any T_{surf}, the temperature profile is linear within the snow cover, as well as the sea ice. Then, the temperature

of each layer of the sea ice cover can be computed .

For the salinity, sea ice type is considered with differentiation between MYI and FYI. For FYI, the salinity is assumed to be homogeneous in the vertical direction, and equal the bulk salinity as prescribed by the sea ice thickness. The bulk salinity for FYI is in turn adapted from the multi-linear structure in Cox and Weeks (1974), and defined as follows (where S_{ice} is in ppt):

$$S_{ice} = 6.08 * e^{(-5.81*h_{ice})} + 7.409 * e^{(-0.5228*h_{ice})} + 1.5$$

With the deepening of the FYI sea ice cover, the bulk salinity decreases, and its minimum value is kept above 1.5 ppt. On the other hand, for MYI, in order to reflect the effect of brine drainage and flushing during the melt season, a vertical salinity profile is adopted following Schwarzacher et al., (1959). For the *k*-th sea ice layer, the mean salinity ($S_{i,k}$) is prescribed as:

$$S_{i,k} = \frac{1}{2} S_{max}[1 - \cos(\pi z^{a/(z+b)})]$$

where *z* is the normalized vertical coordinate with respect to sea ice thickness (starting from 0 on the ice surface to 1 on the ice bottom) and $z = (k - 1/2)/N$, N is number of ice layers, and $S_{max} = 3.2\ ppt$, *a*=0.407, *b*=0.573 which are the fitted parameters from in-situ MYI salinity observations. Therefore, for MYI, the sea ice salinity ranges from 0 at the top of the surface ($z = 0$) to S_{max} at the bottom ($z = 1$). The sea water salinity is fixed at constant $33\ g/kg$.

3. Radiative properties

The radiation model describes the radiation emitted from snow cover, sea ice and sea water, the brightness temperature (TB) at the top of atmospheric (TB_{TOA}) can be described as (Maaß et al., 2013b):

$$TB_{TOA} = (1 - c) * (TB_{water} + (1 - e_{water}) * TB_{cosm}) + c * (TB_{ice} + (1 - e_{ice}) * TB_{cosm}) + \Delta TB_{atm}$$

where c is sea ice concentration, e_{ice} and TB_{ice} the emissivity and TB of sea ice, e_{water} and TB_{water} are the emissivity and TB of sea water, TB_{cosm} is cosmic microwave background radiation, which can be considered as uniform and constant (2.7K). ΔTB_{atm} is TB from atmospheric contribution ranging from -0.36 K and +5.67 K. e_{water} is from the Fresnel equations in different directions of polarization (Ulaby et al., 1981) and e_{ice} is a function of parameters such as polarization, incidence angle, sea ice thickness, temperature, density, salinity, surface roughness, snow depth and temperature, etc.

Based on Maaß et al., (2013a), permittivity of snow (ϵ_{snow}) is determined by a polynomial fit obtained from measurements at microwave frequencies ranging between 840 MHz and 12.6 GHz (Tiuri et al., 1984) as follows:

$$\epsilon_{snow} = (1 + 0.7\rho_{snow} + 0.7\rho_{snow}^2) + i * \left(1.59\times10^6\times(0.52\rho_{snow} + 0.62\rho_{snow}^2)\times(f^{-1} + 1.23\times10^{-14}\sqrt{f})e^{0.036T}\right)$$

where ρ_{snow} is the relative density of snow (compared to water), *T* the temperature of snow in degrees Celsius and f the microwave frequency. It should be noted that ϵ_{snow} depend on snow wetness, which is note considered by the model. Permittivity of sea ice (ϵ_{ice}) is confirmed by brine volume fraction (V_b) using empirical relationship in Vant et al., (1978):

$$\epsilon_{ice} = a_1 + a_2 V_b + i * (a_3 + a_4 V_b)$$

where V_b is given in ‰, and the values of a_1, a_2, a_3, and a_4 following Kaleschke et al., (2010). Similar to Maaß et al. (2013a), for the permittivity of sea water (ϵ_{water}), empirical

relationship from Klein and Swift (1977) is adopted and permittivity of air (ϵ_{air}) is assumed to be 1. The brine volume fraction V_b can be expressed in the following (Cox and Weeks, 1983):

$$V_b = \frac{\rho_{ice} S_{ice}}{\rho_{brine} S_{brine} (1 + k)}$$

where S_{ice} is the ice salinity, ρ_{ice} the ice density, S_{brine} the brine salinity and ρ_{brine} the brine density. ρ_{brine} can be fitted with S_{brine} (Cox and Weeks, 1983):

$$\rho_{brine} = 1 + 0.0008 * S_{brine}$$

where S_{brine} is in ‰. Then the following equation is adopted to relate S_{brine} with T_{ice} (Vant et al., 1978):

$$S_{brine} = a + b * T_{ice} + c * T_{ice}^2 + d * T_{ice}^3$$

where T_{ice} is in ℃ and a, b, c, d are fitted parameters in Vant et al., (1978). These polynomial approximations agreed well with the experimental data of Zubov and Nikolaĭ, (1963).

Also, ρ_{ice} can be expressed by ice temperature (T_{ice}: ℃) in Pounder (1965):

$$\rho_{ice} = 0.917 - 1.403 * 10^{-4} T_{ice}$$

Therefore, V_b can be expressed as a function of ρ_{ice}, S_{ice} and T_{ice}.

As derived model from Burke et al. (1979), the radiation model is a non-coherent model. However, the effect of non-coherency is considered to be mitigated by several factors. First, since with the SMOS observations, there exists large variability of both sea ice thickness and snow depth within the typical resolution of 40 km. Second, multi-angle mean of SMOS TB further introduces a range of integration path of radiations. These factors would enable the use of non-coherent model in this study (RMS of ***Hi*** variation larger than 1/4 of L-band wavelength, as indicated in Kaleschke et al., (2010)). The multi-layer treatment of the sea ice also explored in Maaß et al. (2013b). With treatment of the salinity profile in MYI (i.e., salinity drainage in the top layers), the modeled TB is more consistent with the SMOS TB, as studied in Zhou et al. (2017).

4. Modeled TB under typical sea ice parameters

Under typical winter Arctic conditions (surface temperature is −30℃), simulated brightness temperature (TB) over different sea ice type from reformulated radiation model shows in Figure S1, along with snow freeboard contour.

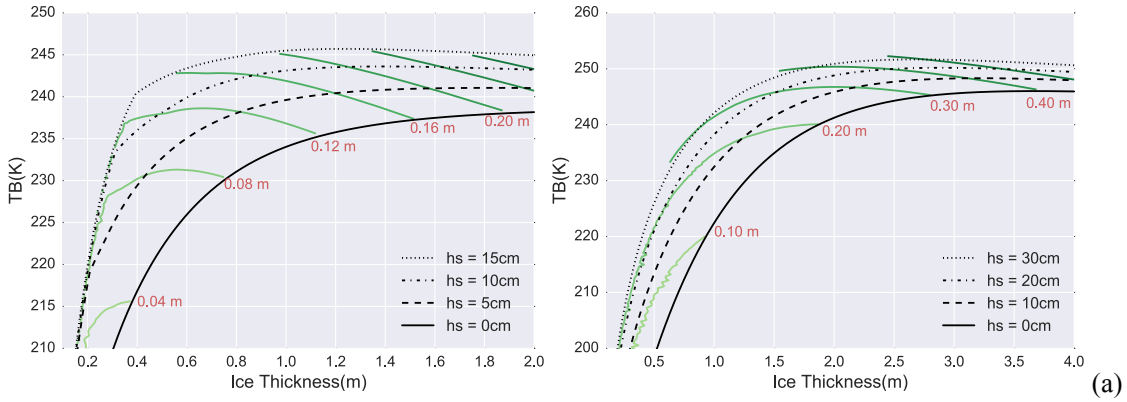

Figure S1. Simulated sea ice surface TB based on reformulated radiation model over FYI (a) and MYI (b). Colored lines are snow freeboard isolines.

5. Supportive information for the verification with OIB and SMOS data

Verification is carried out between OIB data and SMOS, with specific attention to the effect of better OIB sampling. Due to the resolution difference between SMOS and OIB (or any type of satellite altimetry), we consider multiple (M) OIB samples correspond to a single SMOS TB. Figure 2 of the manuscript provides a corresponding relationship between the two. Figure S2 shows the distribution of M, using all OIB data. The mean value of M is about 700. The RMSE of TB (modeled v.s. observed) is 3.1 K for all available OIB data (see also Figure 3.b of the manuscript). If we further limit the computation of RMSE to the points with large values of M (95-percentile for M, corresponding to areas with good OIB coverage), the RMSE drops to 1.41 K. Figure S3 shows the relationship of RMSE of TB and M. As shown, there exists drop in both RMSE and the maximum error of TB with better spatial coverage of OIB.

The integration of lead information is explored in Zhou et al. (2017), which effectively reduces the overestimation of TB as caused by refrozen leads or open water.

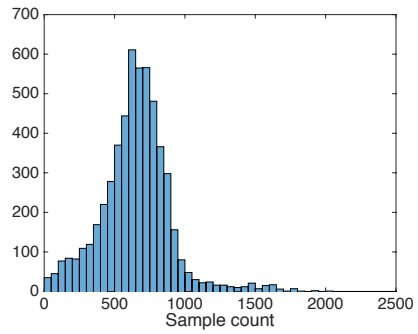

Figure S2. Distribution of OIB sample count (M).

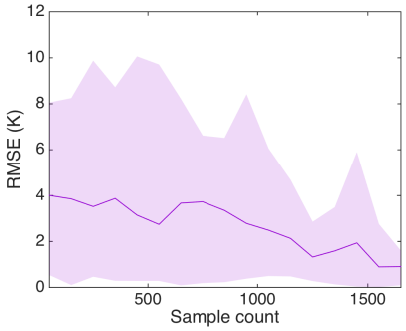

Figure S3. The relationship of RMSE of TB to OIB sample count (M).
The statistics of RMSE of TB are computed for each sample count bin (each of 100).
Shaded area covers the 5-th and 95-th percentile of the absolute TB error.

References:

Burke W J, Schmugge T, Paris J F. Comparison of 2.8-and 21-cm microwave radiometer observations over soils with emission model calculations[J]. Journal of Geophysical Research: Oceans, 1979, 84(C1): 287-294.

Cox G F N, Weeks W F. Salinity variations in sea ice[J]. Journal of Glaciology, 1974, 13(67): 109-120.

Cox G F N, Weeks W F. Equations for determining the gas and brine volumes in sea-ice samples[J]. Journal of Glaciology, 1983, 29(102): 306-316.

Maaß N, Kaleschke L, Tiankunze X, et al. Snow thickness retrieval over thick Arctic sea ice using SMOS satellite data[J]. Cryosphere, 2013a, 7(6):1971-1989.

Maaß N, Kaleschke L, Stammer D. Remote sensing of sea ice thickness using SMOS data[D]. University of Hamburg Hamburg, 2013b.

Maykut G A, Untersteiner N. Some results from a time-dependent thermodynamic model of sea ice[J]. Journal of Geophysical Research, 1971, 76(6): 1550-1575.

Kaleschke L, Maaß N, Haas C, et al. A sea-ice thickness retrieval model for 1.4 GHz radiometry and application to airborne measurements over low salinity sea-ice[J]. The Cryosphere, 2010, 4(4): 583-592.

Klein L, Swift C. An improved model for the dielectric constant of sea water at microwave frequencies[J]. IEEE Journal of Oceanic Engineering, 1977, 2(1): 104-111.

Pounder, E.: The Physics of Ice, Pergamon Press, the Common- wealth and International Library, Geophysics Division, Oxford, 1965.

Schwarzacher W. Pack-ice studies in the Arctic Ocean[J]. Journal of Geophysical Research, 1959, 64(12): 2357-2367.

Tiuri M, Sihvola A, Nyfors E, et al. The complex dielectric constant of snow at microwave frequencies[J]. IEEE Journal of Oceanic Engineering, 2003, 9(5):377-382.

Ulaby F T, Moore R K, Fung A K. Microwave remote sensing: Active and passive. volume 1-microwave remote sensing fundamentals and radiometry[J]. 1981.

Untersteiner N. Calculations of temperature regime and heat budget of sea ice in the central Arctic[J]. Journal of Geophysical Research, 1964, 69(22): 4755-4766.

Vant M R, Ramseier R O, Makios V. The complex-dielectric constant of sea ice at frequencies in the range 0.1–40 GHz[J]. Journal of Applied Physics, 1978, 49(3):1264-1280.

Yu Y, Rothrock D A. Thin ice thickness from satellite thermal imagery[J]. Journal of Geophysical Research: Oceans, 1996, 101(C11): 25753-25766.

Zhou L, Xu S, Liu J, et al. Improving L-band radiation model and representation of small-scale variability to simulate brightness temperature of sea ice[J]. International Journal of Remote Sensing, 2017, 38(23): 7070-7084.

Zubov, Nikolaĭ Nikolaevich. Arctic ice. Naval Oceanographic Office Washington DC, 1963.

Part 2: Statistics for the covariability between FB_s and *hs*

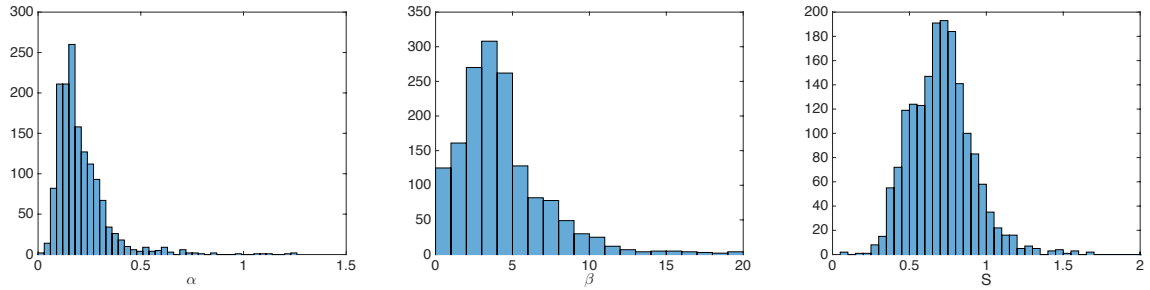

(a) ***alpha***. (b) ***beta***. (c) ***s***.

Figure S4. Distribution of alpha, beta and s for FYI. 40-meter resolution (OIB) data are used for computing the value of each parameter on the scale of 37.5 km (i.e., approximately native resolution of SMOS TB)

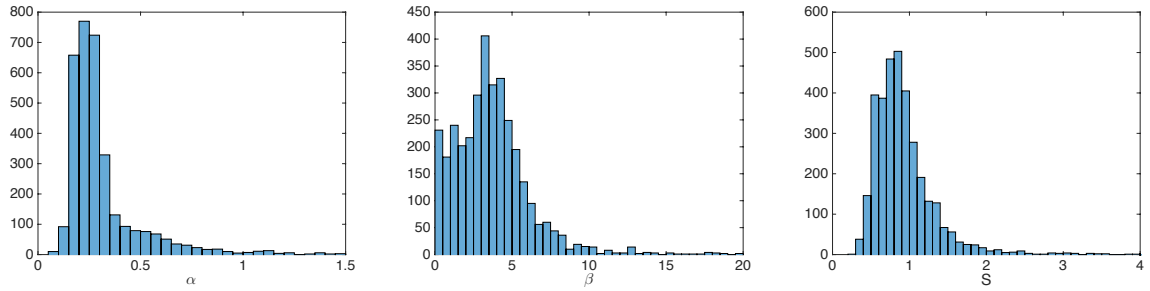

(a) ***alpha***. (b) ***beta***. (c) ***s***.

Figure S5. Distribution of alpha, beta and s for MYI. Specifications are the same as Figure S4.

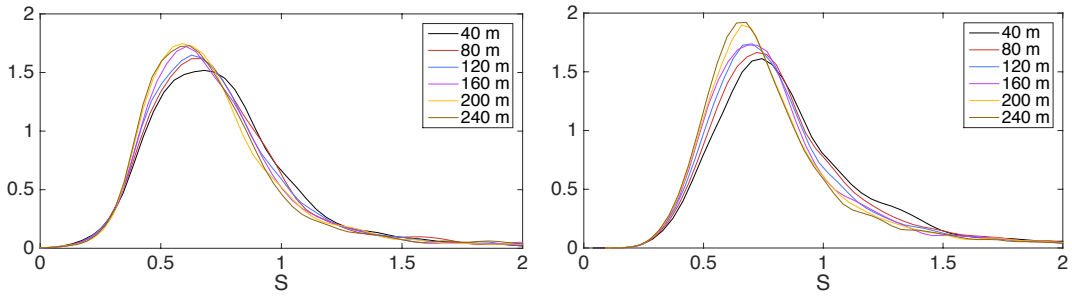

(a) FYI. (b) MYI.

Figure S6. Scaling of ***s*** derived from OIB data. PDFs of ***s*** are shown.